AF 61 (052)-576
ASR - 3
March 1965

TECHNION RESEARCH & DEVELOPMENT
FOUNDATION HAIFA, ISRAEL

ANNUAL SUMMARY REPORT No. 3

NEAR WAKE FLOW STUDIES IN SUPERSONIC FLOW

by

Josef Rom

Technion - Israel Institute of Technology

Department of Aeronautical Engineering

Haifa, Israel

TAE REPORT No. 38

AF 61 (052) – 576
ASR – 3
March 1965

ANNUAL SUMMARY REPORT No. 3

NEAR WAKE FLOW STUDIES IN SUPERSONIC FLOW

by

Josef Rom
Technion – Israel Institute of Technology
Department of Aeronautical Engineering
Haifa, Israel

TAE REPORT No. 38

The research reported in this document has been sponsored by the Aerospace Research Laboratories, OAR, through the European Office of Aerospace Research, United States Air Force.

SUMMARY

The theoretical and experimental investigations carried out under contract AF 61(052) – 576 on supersonic flow over two-dimensional and axially symmetric base type separated flows are summarized in this report.

Correlating equations for base pressure and backward facing step pressure with laminar and turbulent separation are presented. These relations are obtained from considerations of the analysis based on the integral method and experimental data.

Measurements of total pressure and temperature profiles in the near wake of a two-dimensional wedge-flat plate model at $M = 3.5$ indicate high recovery temperatures at the outer regions of the wake beyond the "neck" position.

The development of the shock tunnel and its associated equipment is reported, including an improved method for thin film resistance thermometers calibration.

TABLE OF CONTENTS

LIST OF SYMBOLS

a	–	speed of sound
a_t	–	speed of sound at stagnation temperature conditions
C	–	specific heat of solid
$C(\kappa)$	–	mixing rate correlation function
$\bar{C}$	–	average value of laminar $C(\kappa)$ between separation and shock impingement positions
$\bar{C}_t$	–	average value of turbulent $C(\kappa)$ between separation and shock impingement positions
D	–	forebody diameter
E	–	electrical potential difference
$F(\kappa)$	–	momentum correlation function
h	–	base height
I	–	momentum flux
k	–	thermal conductivity
L	–	length of fore body ahead of step
$\bar{m}$	–	mass flux in the x direction
m	–	$\bar{m}a_t$
M	–	Mach number
p	–	pressure
q	–	heat transfer rate
Re	–	Reynolds number
R	–	electrical resistance
S	–	film active area
T	–	temperature

t	–	time
u	–	velocity in the x direction
ΔV	–	voltage signal across gage
x, y	–	coordinates along a normal to body axis
x	–	distance measured from step position
x_{sh}	–	distance between base and beginning of reattachment
x_r	–	distance between base and end of reattachment
α	–	thermal resistivity
γ	–	specific heat ratio
δ	–	thickness of viscous layer
δ^*	–	displacement thickness
δ^{**}	–	momentum thickness
κ	–	Crocco-Lees velocity profile shape parameter
ρ	–	density

SUBSCRIPTS

b	–	base conditions, or belonging to backing material
e	–	external flow conditions
f	–	instantaneous film conditions
i	–	incompressible conditions
l	–	laminar conditions
s	–	separation point conditions
sh	–	shock impingement position conditions
t	–	turbulent condition
0	–	undisturbed flow conditions upstream of separation, or initial conditions
∞	–	conditions far downstream of base.

LIST OF FIGURES

I. INTRODUCTION

The present report summarizes the results of the third year of research on wakes and separated flows under contract AF 61(052)-576. Various results of this investigation are presented in References 1 to 10.

The research program is aimed at studies of base type separated flows in supersonic and hypersonic speeds with particular emphasis on heat transfer effects. The theoretical analysis of the laminar separated flows is based on the Crocco-Lees theory (Ref. 11) and on the modification of this theory which was introduced by Glick (Ref. 12). The problem of the turbulent separated flow is treated by a similar procedure based on the general similarity between laminar and turbulent separated flows (Refs. 6, 8 and 9). The results of these analyses and the comparison with experimental data are summarized in Ref. 9.

The main results presented in Ref. 9 are discussed in Parts II and III of the present report. Further results of the research on axially symmetric base type separated flows are discussed in Part IV. Experiments with "large diameter" models are described and some preliminary results are presented. Measurements of total and static pressure profiles and total temperature profiles in the near wake behind a two-dimensional model are discussed in Part V. The shock-tunnel and its associated instrumentation is described in Part VI. A calibration method for the thin film resistance thermometers is described as well as an analog circuit for direct evaluation of the heat transfer rate.

II. SEPARATED FLOWS ANALYSIS

A. THE KORST-CHAPMAN ANALYSIS

It is assumed that the separated flows can be divided into distinct regions, as indicated in Fig. 1. The dominating effect of this flow field is assumed to be due to the shear layer which extends from the separation point to reattachment. This free shear layer is divided into an "external" flow and a "dead air" region by the "dividing" streamline (Fig. 1). The Korst-Chapman criterion postulates that the total pressure on the dividing streamline must equal the "downstream"-(reattachment) pressure of

the external flow. The streamlines under the "dividing"-streamline must have lower total pressure and therefore are reversed into the "dead-air" region. The velocity on the dividing streamline is calculated assuming similar velocity profiles in the free shear layer. Using this basic model Korst (Refs. 13 and 14) has outlined the solution for the base pressure for a variety of separated flows. Considering the flow over a two-dimensional backward facing step, the solution can be found by matching the total pressure on the "dividing"-streamline with the pressure rise either across the oblique shock wave or through an isentropic recompression at reattachment. The pertinent parameters are shown in Fig. 1. Once the ratio of the "dividing" streamline is determined and this ratio is assumed to be independent or Reynolds number then the base pressure is found to be a function only of the flow Mach number just ahead of the step. This base pressure variation as a function of the flow Mach number for turbulent flows is shown in Fig. 2. Chapman, in Ref. 15, applied a similar flow model to the case of laminar separation, assuming that the total pressure on this "dividing streamline" is matched by the pressure obtained by an isentropic recompression at reattachment.

The Korst-Chapman analysis assumed, in the calculation of the shear layer velocity profiles, zero thickness boundary layer at separation. It is then implied that such a solution is a fairly good approximation for cases when δ_s/h is very small. This solution is based on the realization that in the limit of $\delta_s \to 0$, the flow field and thus the base pressure are independent of the Reynolds number. In many practical problems the boundary layer at separation may be small, compared to step height, but not negligible. In such cases the experimental results (References 4, 6, 8 and 16 to 23), shown in Fig. 2, do indicate a marked Reynolds number effect. Various attempts to modify the Korst-Chapman theory to introduce effects of initial boundary layer thickness were presented by Nash (Ref. 24) for the turbulent case and by Denison and Baum (Ref. 25) and by Kabota and Dewey (Ref. 26) for the laminar case.

For the turbulent separation case, Nash (Ref. 24) introduces an empirical factor N, which is the ratio of the actual pressure rise at the reattachment point, found in experimental results, to the overall pressure rise estimated by the Korst-Chapman theory. Using this empirical factor, the base pressure for turbulent separation is found to be a function of δ_s^{**}/h.

In the laminar separation case, the velocity on the dividing streamline can be determined analitically. Chapman (Ref. 15) found the value of $u^* = 0.58$ for incompressible flow in the limiting case of zero initial boundary layer thickness (where $u^* = u/u_e$ on the dividing streamline) Denison and Baum

(Ref. 25) and Kabota and Dewey (Ref. 26) showed that u^* is a function of Mach number and a viscous parameter $(\nu l/\delta^{*2} u_e)$ where l is the distance along the free shear layer. Since δ^* is proportional to $(\nu l/u_e)$, it is found that the value of u^* is again independent of free stream Reynolds number. Thus far, these attempts to account for the Reynolds number effect in laminar shear layers were not very successful. The existence of a marked Reynolds number effect can be seen in the experimental data presented in Refs. 2 and 16 to 21.

The Korst-Chapman theory does not account for the viscous effects at reattachment. Thus reattachment in the case of backward facing step and free wake are both treated as being inviscid. The reattachment behind a backward facing step may be assumed to be inviscid due to its relatively short length. The recompression in the wake is much more gradual and involves the refill of the wake mass flow introduced into the recompression zone by mixing. This process is radically different from that when the reattachment is on a solid surface and it is questionable whether these cases can be treated identically. However, the similarity in the order of the separated pressures in the blunt base case and the backward facing step, as well as in the case of the corresponding axially symmetric configurations, may lead to approximations which predict the order of magnitude of the base pressure but in which some basic physical mechanisms are neglected. Such approximations may not distinguish between some of the qualitative differences between the various separated flows. It will be shown that the effect of reattachment flow conditions are important and can be included in the momentum integral methods.

B. THE MOMENTUM INTEGRAL METHODS

The technique of integration of the boundary layer equations across the boundary layer in order to obtain relations between the overall physical parameters, when details of velocity distribution and/or exact skin friction laws are not known, is a powerful tool introduced by Von Karman and Pohlhousen as a boundary layer approximate analysis (Ref. 27). The application of this method to the separated flow case was presented by Crocco and Lees (Ref. 11). The flow field is found to be governed by few correlating functions defined from the integral relations. These functions must be determined by either independent analysis or by empirical data. Some of the considerations for evaluation of these functions, which were presented in Ref. 11, were found to be erroneous. It was later shown in Ref. 12 that with suitable choice of the correlating functions the separated flow generated by the interaction of a shock

wave and a laminar boundary layer can be correctly evaluated. Applications of the momentum integral method, using some of the correlating functions which were introduced in Ref. 12, for the analysis of laminar base type flows were presented in Ref. 1. The dependence of the base pressure on Reynolds number was then explicitely obtained through the effect of Reynolds number on the mixing rate as shown in Refs. 1, 2 and 6. In the calculation of the pressure immediately behind a backward facing step presented in Refs. 2 and 6 one parameter is left to be determined empirically. This parameter is the mixing rate coefficient. Its value in the laminar mixing over a backward facing step was found in Ref. 2 to agree well with the value found by Glick (Ref. 12) for the shock wave boundary layer interaction.

The flow conditions in the reattachment zone, in the case of a backward facing step, or recompression zone, in the case of a blunt base, can be explicitly described in the integral method formulation through the different variations of the correlating function in these zones. Thus, the dependence of the flow field and base pressure on the reattachment or recompression condition is explicitly obtained.

The use of integrals of higher moments of the momentum equation may enable further insight into the separated flow field as discussed by Lees and Reeves in Ref. 28. Effects of heat transfer, as well as mass addition, may also be introduced into the integral method formulation through the use of the suitable continuity, momentum and energy integral equations.

III. THE INTEGRAL EQUATIONS FOR TWO-DIMENSIONAL BASE TYPE SEPARATED FLOWS

The application of the integral method to the dissipative region in separated flows is discussed in Refs. 1, 11 and 12. Using the usual boundary layer approximation and assumption, the integral equations become:

Continuity Equation

$$d\bar{m} = \rho_e u_e (d\delta/dx - \theta) = \rho_e u_e k \tag{1}$$

Momentum Equation

$$dI/dx = u (d\bar{m}/dx) - (dp/dx) - \tau_0 \tag{2}$$

where τ_0 is the shear stress on the streamline where $u = 0$.

In the nearly isentropic external flow the usual inviscid Bernoulli's equation and the Prandtl-Meyer relations are applicable.

A momentum defect parameter is now defined

$$\kappa = \frac{I}{\bar{m}u_e} = \frac{\delta - \delta^* - \delta^{**}}{\delta - \delta^*} = \frac{\delta_i - \delta_i^* - \delta_i^{**}}{\delta_i - \delta_i^*} \tag{3}$$

and the correlating functions $F(\kappa)$ and $C(\kappa)$ are defined by

$$F(\kappa) = \frac{\delta^* + \delta^{**}}{\delta - \delta^* - \delta^{**}} = \frac{\delta_i^* + \delta_i^{**}}{\delta_i - \delta_i^* - \delta_i^{**}} \tag{4}$$

and

$$C(\kappa) = \frac{k\bar{m}}{\mu_e} = \frac{k_i \bar{m}_i}{\mu_t} \tag{5}$$

It is shown in Ref. 6 that through the use of Stewartson transformation the values of κ, $F(\kappa)$ and $C(\kappa)$ can be determined from the equivalent incompressible solutions. The equivalent incompressible expressions for these functions are also indicated in equations (3), (4) and (5).

The momentum equation can now be written in terms of κ and $F(\kappa)$. The friction term τ_0 is assumed to be much smaller than either the pressure of the mixing terms in the dissipative region and is neglected. The momentum equation is then

$$d\kappa/dx = [(1 - \kappa)/m]\, dm/dx + (\kappa F/M_e)\, (dM_e/dx) \tag{6}$$

Equation (6) is just a restatement of the integral momentum equation, Eq. (2), neglecting the friction stresses. This momentum equation is applicable to both laminar and turbulent separated flows. However, the functional relations of $F(\kappa)$ and $C(\kappa)$ must be known from some independent considerations in order that Eq. (6) may be solved. In lieu of exact knowledge of these functions, approximate functional relations are assumed and used in Refs. 1, 4, 8 and 12 in treating the problem of laminar and turbulent base type flows and that of separation due to shock wave-laminar boundary layer interaction, respectively.

A. FLOW OVER A TWO-DIMENSIONAL BACKWARD FACING STEP

The flow over a backward facing step can be subdivided into the following zones (Fig. 3): (1) Undisturbed flow ahead of step (2) Expansion fan at the step corner, resulting in the sharp drop to the "base-pressure" level. (3) A mixing zone with constant static pressure – the so called "dead-air" zone. Its length, measured from the step, is designated here as x_{sh}. (4) The recompression zone, in which the pressure increases back to the pressure just ahead of the step. Its length is designated here as $(x_r - x_{sh})$. (5) Reestablished flow over the flat surface downstream of the separated region.

Measured pressure distribution on such models both with laminar and turbulent separation indeed confirm the above description. Sample measured pressure distribution, presented in References 2 and 6, for the laminar and turbulent separation cases respectively, are shown in Figs. 4a and 4b.

The momentum integral representation can now be applied to this flow model. Since the laminar and turbulent correlation functions are different, the analysis of these separated flows will be considered in the following sections.

1. LAMINAR SEPARATION

Measurements of the laminar pressure distribution at Mach numbers 2.25 and 3.55 on various models are presented in References 2 and 4. A schematic drawing of the model used in these experiments, with its pressure holes location is shown in Fig. 5. A typical measured pressure distribution is shown in Fig. 4a. The flagged points in Fig. 4a correspond to pressures measured at the points 21 and 22 which are off the center line as indicated in Fig. 5. The base pressure is found to correlate with the parameter $L/h\,Re_L^{1/4}$ as shown in Fig. 6. The distance $\Delta x_{sh}/L$ can also be correlated by the parameter $L/h\,Re_L^{1/4}$ (Ref. 9). Furthermore, these measurements indicate that $\Delta x_{sh}/L$ is a function only of the parameter $L/h\,Re_L^{1/4}$ and does not vary with flow Mach number (within the scatter of the data experienced in the evaluation of Δx_{sh}). This variation can be represented by the empirical relation

$$\Delta x_{sh}/L = 0.0085\,(h\,Re_L^{1/4}/L) \qquad 0.05 < \Delta x_{sh}/L < 0.6 \tag{7}$$

The base pressure will then be only a function of $L/h\,Re_L^{1/4}$ as indicated in Eq. (8). Preliminary exper-

iments in this laboratory with curved forebody shapes ahead of the step, show that this pressure is independent of the forebody shape.

The step pressure is then found to be (Ref. 9)

$$\frac{p_b}{p_0} = \left[\frac{\{1 + [(\gamma-1)/2] M_0^2\}\{0.70/1 - 0.30\,[1 + 0.54\,(h Re_L^{1/2}/L)]^{-1/2}\}^{1.33}}{\{0.70/1 - 0.30\,[1 + 0.054\,(h Re_L^{1/2}/L)]^{-1/2}\}^{1.33} + [(\gamma-1)/2]\, M_0^2} \right]^{\gamma/\gamma-1} \tag{8}$$

In the case of hypersonic flows when $M_0 \gg 1$ the step pressure is given by

$$p_b/p_0 = [0.7/1 - 0.3\,[1 + 0.054\, h Re_L^{1/2}/L]^{-1/2}]^{4.65} \tag{9}$$

The results of Equations (8) and (9) are shown in Fig. 6. Included are the experimental results which are the basis for this semi-empirical correlation.

2. TURBULENT SEPARATION

The flow field in the case of turbulent separation is described in Fig. 3. This flow structure is qualitatively similar to the laminar one, as can be seen by comparing the pressure distributions presented in Figs. 4a and 4b. The qualitative similarity between the structure of laminar and turbulent separated flows has been discussed by Chapman in Ref. 16. Using the assumption that the turbulent separated flows are qualitatively similar to the laminar ones, except for the much higher mass mixing rate in the turbulent case, it is shown in Ref. 9 that the step pressure is then

$$\frac{p_b}{p_0} = \left[\frac{\{1 + [(\gamma-1)/2] M^2\}\,[0.89/1 - 0.11\,(1 + 19 Re_L^{-3/5}\, \bar{C}_t\, \Delta x_{sh}/L^{-1/17}]^{7}}{[0.89/1 - 0.11\,(1 + 19 Re_L^{-3/5}\, \bar{C}_t\, \Delta x_{sh}/L)^{-1/17}]^{7} + [(\gamma-1)/2]\, M_0^2} \right]^{\gamma/\gamma-1} \tag{10}$$

In the limiting case of the incoming boundary layer thickness approaching zero, $L \to 0$ the limiting base pressure is

$$\frac{p_b}{p_{0_{L\to 0}}} = \left[\frac{0.442\,\{1 + [(\gamma-1)/2]\, M_0^2\}}{[(\gamma-1)/2]\, M_0^2 + 0.442} \right]^{\gamma/(\gamma-1)} \tag{11}$$

This limiting pressure is compared with Korst calculations for the very thin boundary layers in Fig. 2. This result is about 30% below the Korst values at the low supersonic Mach numbers and seems to be a lower limit for the measured base pressures.

Measurements of the turbulent pressure distributions at Mach number 2.25 and 3.5 on various step models are presented in Refs. 6 and 8. The models are similar to the models used in the laminar flow experiments shown in Fig. 5, except for the longer flat plate ahead of the step and the deeper steps. A typical measured pressure distribution is shown in Fig. 4b. The flagged points here denote again pressures measured at points 21 and 22, as indicated on Fig. 5. The base pressure is found to be correlated by the parameter $(Re_L^{-3/5} \Delta x_{sh}/L)$. The mixing zone length $\Delta x_{sh}/L$ is found to be, in the turbulent case, independent of Mach number and Reynolds number. The empirical relation for $\Delta x_{sh}/L$, determined in Ref. 9, is

$$\Delta x_{sh}/L = 1.8\,(h/L) \tag{12}$$

The correlation of the base pressure with the parameter $(Re_L^{-3/5} h/L)$ is shown in Fig. 7. The value of $\bar{C}_t$ is found in Ref. 9 to be equal to $\bar{C}_t = 27.3 \times 10^3$. The base pressure is then

$$\frac{p_b}{p_0} = \left[\frac{\{1 + [(\gamma-1)/2]\, M_0^2\}\,[0.89/1 - 0.11\,(1 + 9.33 \times 10^5\, Re_L^{-3/5} h/L)^{-1/4}]^7}{[0.89/1 - 0.11\,(1 + 9.33 \times 10^5\, Re_L^{-3/5} h/L)^{-1/4}]^7 + [(\gamma-1)/2\, M_0^2]} \right]^{\gamma/\gamma-1} \tag{13}$$

Comparison of the equations for the mass addition in the laminar and turbulent cases, shows that the mass addition in the turbulent experiments reported here, where Re_L varies between 0.5×10^6 to 4×10^6, is larger than the laminar one by a factor of 2 to 6. In addition, the low value of the turbulent F_s compared to the laminar value – 2/7 compared to 1.55 – results in a much lower turbulent base pressure. The turbulent correlating parameter $(Re_L^{-3/5} h/L)$ can be interpreted in terms of the ratio of the incoming boundary layer thickness to step height as follows: $(Re_L^{-3/5} h/L) = h/(\delta \cdot Re_L^{4/5})$. Eq. (13) indicates that at a fixed Mach number the pressure behind a backward facing step should increase with increasing Reynolds number when the separation is fully turbulent. Experimental data found in this laboratory tend to confirm this result. Published data presented in References 16, 18, 20 and 22 tend to confirm this variation of step pressure with flow Reynolds number. The ques-

tion always exists if this pressure variation is not due to transition effects when the incoming boundary layer is not fully turbulent. Some of the tests were performed with artificial boundary layer trips in order to insure transition well ahead of the step. In these cases as well, the pressure just behind the step is found to increase with increasing Reynolds number. The Reynolds number ranged in these tests between 1×10^6 to 5×10^6 at Mach number of 2.25. At these conditions one expects fully turbulent boundary layers. Additional data at higher separation Reynolds number may still be informative. At this time no such data is available at this laboratory due to limitation on wind-tunnel model size and wind-tunnel working pressure.

a. Effect of Step Cavity with Turbulent Separation

A preliminary investigation as to the effect on the separated region parameters of a cavity at the step face was undertaken*. A backward facing step model of basic step height of $h = 2$ mm is modified by bonding a 0.2 mm bronze sheet to the upper surface leaving an overhange as shown in Fig. 5(b). The overhange lengths used are 3.5 mm, 1.1 mm and 0.35 mm with a step height of 2.2 mm. The pressure distribution is measured by the available pressure holes on the model. The step pressure and the separation region lengths Δx_{sh} and Δx_r are found to be unaffected by the presence of the cavity. These pressure measurements are shown in Fig. 7.

B. FLOW OVER A TWO-DIMENSIONAL BASE

The flow over a two-dimensional base can be divided into the following zones (Fig. 8); (1) Undisturbed flow ahead of the base. (2) Expansion fan at the base, resulting in the sharp pressure drop to the base pressure level. (3) A mixing zone with essentially constant static pressure – the so-called "dead-air" zone. (4) Recompression zone, in which the pressure increases slowly back to its undisturbed value ahead of the base and uniform flow conditions are re-established. Available experimental data tend to confirm this flow model. There is a reasonable collection of the pressure data so that the analytical results can be judged by their applicability to the available base pressure data. Here again the laminar and turbulent cases will be discussed separately.

* This investigation was suggested by Dr. M. Scherberg of ARL.

1. LAMINAR SEPARATION

In this base type flow, the boundary layer is assumed to be undisturbed up to the separation point at the base. The adjustment to the base pressure, following the Prandtl-Meyer expansion fan, is assumed to be accomplished within a very short distance, so that the constant pressure mixing zone extends from x_s to x_{sh} (Fig. 10). The integral momentum equation for this region is identical to that for the uniform pressure laminar mixing zone over a backwards facing step. The mass mixing rate dm/dx in this flow is caused by the mixing layers below and above the center line. These shear layers do interact. Preliminary calculations show that when the mass mixing rate in the mixing zone behind the base is assumed to be twice the mass mixing rate to the backward facing step mixing zone, then the calculated base pressure is too low for thin incoming boundary layers and too high for relatively thick incoming boundary layers. The correct analytical relation for this mixing rate is not known at this time. An empirical relation for m_{sh}/m_s can be inferred from available experimental data. The base pressure can then be evaluated as a function of this mass mixing parameter.

In the recompression zone the pressure increases slowly to its value ahead of the base, w the velocity defect existing in the "dead-air" zone is filling up towards a uniform velocity far downstream of the base. In terms of the integral functions this behaviour is described by the momentum defect parameter increasing to 1 and the energy defect parameter F decreasing towards 0 (Ref. 1). Wh the parameter $\delta/h \approx L/h\,Re_L^{1/2}$ is relatively small the value of κ_{sh} is approaching 1. So, if we exclude the case of very thick boundary layers compared to base height, then the effect of the increase in κ, from its value of κ_{sh} towards 1, must be much smaller than either the mixing or the pressure contribution in the integral momentum equation. In this case the integral momentum equation is

$$dM_e/M_e = -[(1-\kappa)/\kappa F]\ (dm/dx) \qquad (14)$$

The value of $F(\kappa)$ in the far wake is evaluated in Ref. 1 to be approximately

$$F(\kappa) = -2(1-\kappa) \qquad \text{for } \kappa \to 1 \tag{15}$$

Eq. (14) can then be integrated between x_{sh} and x_∞

$$M_\infty/M_{sh} = (m_{sh}/m_\infty)^{1/2} = (m_{sh}/m_s)^{1/2}(m_s/m_\infty)^{1/2} \tag{16}$$

as discussed previously, the value of m_{sh}/m_s must be found from empirical data.

The value of m_∞, which is the mass flow in the wake after recompression, can be evaluated by the following procedure. The flow conditions in the far wake after recompression are again nearly uniform. Therefore, the mass flow far downstream, m_∞; and the mass flow at separation, m_s, are respectively (Ref. 1):

$$\bar{m}_\infty = \rho_e u_e (h + 2\delta_s^*)$$

and (17)

$$\bar{m}_s = 2\rho_s u_s (\delta_s - \delta_s^*)$$

Since $m_i = m = \bar{m}a_t$ (Ref. 11) the value of m_s/m_∞ can be evaluated from the incompressible Blasius boundary layer velocity profile at separation (δ_i is defined at $u_i/u_{i_e} = 0.95$)

$$(m_s/m_\infty) = 2(\delta_{s_i} - \delta^*_{s_i})/(h + 2\delta^*_{s_i}) = 4.53/[(hRe_L^{1/2}/L) + 3.40] \tag{18}$$

The base pressure is then

$$\frac{p_b}{p_0} = \left[\frac{\{1 + [(\gamma - 1)/2]\, M_0^2\}\,(m_{sh}/m_s)\, 4.53/[(hRe_L^{1/2}/L) + 3.40]}{(m_{sh}/m_s)\, 4.53/[(hRe_L^{1/2}/L) + 3.40] + [(\gamma - 1)/2]\, M_0^2}\right]^{\gamma/\gamma-1} \tag{19}$$

The base pressure measurements presented in Refs. 15, 17, 18 and 19 can be used for evaluation of (m_{sh}/m_s) by the use of Eq. 19 as a function of $L/hRe_L^{1/2}$. The values of $(m_{sh}/m_s)_1$ thus evaluated from this data in the Mach number range of 1.5 to 4 are shown in Fig. 9. An empirical relation can then be obtained between $(m_{sh}/m_s)_1$ and $L/hRe_L^{1/2}$

$$(m_{sh}/m_s)_1 = 0.45 \cdot (L/hRe_L^{1/2})^{-3/4} \tag{20}$$

The laminar base pressure can then be evaluated by

$$\frac{p_b}{p_0} = \left[\frac{\{1 + [(\gamma - 1)/2]\, M_0^2\}\, 2.0\,(hRe_L^{1/2}/L)^{3/4}\,(hRe_L^{1/2}/L + 3.40)^{-1}}{2.0\,(hRe_L^{1/2}/L)^{3/4}\,(hRe_L^{1/2}/L + 3.40)^{-1} + [(\gamma - 1)/2]\, M_0^2}\right]^{\gamma/\gamma-1} \tag{21}$$

The base pressure evaluation by Eq. (21) is plotted in Fig. 10 as a function of $hRe_L^{1/2}/L$ for various flow Mach numbers. The experimental results of the cited references (Refs. 16, 17, 18 and 19) are indicated on this figure. It can be seen that within the scatter of experimental data the correlation of Eq. 21 is reasonable in accounting for the Mach number and Reynolds number effects.

2. TURBULENT SEPARATION

The flow model that can be used in the description of this flow is basically similar to the laminar one as shown in Fig. 8. In the uniform pressure mixing zone, extending between x_s and x_{sh}, the basic integral momentum equation is similar to that of the laminar case (Ref. 9). Here again the base mixing is expected to be influenced by the interaction between the shear layers as in the laminar

case discussed previously. Therefore, the actual mixing in the base region $(m_{sh}/m_s)_t$ should be determined from experimental data.

The recompression zone can be dealt here similarly to the case of the laminar wake in the previous section. The pertinent equations are then (14), (15), (16) and (17).

The relation for mass flow in the far wake becomes in this case

$$(m_s/m_\infty)_t = 2(\delta_{s_i} - \delta^*_{s_i})/(h + \delta^*_{s_i}) = 0.668/[(h\,Re_L^{1/5}/L) + 0.095]$$

The turbulent base pressure is given by

$$\frac{p_b}{p_0} = \left[\frac{\{1 + [(\gamma - 1)/2]\,M_0^2\}\,(m_{sh}/m_s)_t\;0.668/[(h\,Re_L^{1/5}/L) + 0.095]}{(m_{sh}/m_s)_t\;0.668/[(h\,Re_L^{1/2}/L) + 0.095] + [(\gamma - 1)/2]\;M_0^2}\right]^{\gamma/\gamma-1} \tag{22}$$

Measured turbulent base pressure presented in References 17 and 18 and additional data obtained at this laboratory can be used in order to determine m_{sh}/m_s from Eq. 22. The variation of the turbulent m_{sh}/m_s as a function of $L/h\,Re_L^{1/5}$ is shown in Fig. 11 using experimental results obtained at flow Mach numbers varying between 1.5 and 4.0. An empirical relation can then be obtained from m_{sh}/m_s

$$m_{sh}/m_s = (h\,Re_L^{1/5}/L)^{0.85} \tag{23}$$

and the base pressure can be written then as

$$\frac{p_b}{p_0} = \left[\frac{\{1 + [(\gamma - 1)/2]\,M_0^2\}\,\{0.668\,(h\,Re_L^{1/5}/L)^{0.85}\,[(h\,Re_L^{1/5}/L) + 0.095]^{-1}\}}{0.668\,(h\,Re_L^{1/5}/L)^{0.85}\,[(h\,Re_L^{1/5}/L) + 0.095]^{-1} + [(\gamma - 1)/2]\;M_0^2}\right]^{\gamma/\gamma-1} \tag{24}$$

The base pressure evaluated by Eq. 24 is shown in Fig. 12. The experimental results of the cited references are indicated in this figure as well. Here again the Mach and Reynolds number effects are clearly described by the semi-empirical relation (Eq. 24), with good agreement with the experimental results over the range of parameters obtained in the experiments.

IV. AXIALLY SYMMETRIC BASE TYPE SEPARATED FLOWS

The axially symmetric base type separated flows are governed by the interaction of the viscous

mixing with the external inviscid flow. The differences between the axially symmetric separated flows and the two-dimensional ones are due to the curvature of the external streamlines, which is caused by the corresponding curvature of the axially symmetric supersonic characteristic lines, due to the "squeezing" effect on the centerline of the axially-symmetric recompression zone. It can be then anticipated that the number of parameters required to define the axially-symmetric flows must be larger than in the case of two-dimensional flows. The flow characteristics and the geometry may be used to define the following parameters: M_0, $2h/D$, $2\delta/D$, and L/D in case of an axially symmetric backward facing step and M_0, L/D and $2\delta/D$ in case of an axially symmetric base. It should be noted that in the two dimensional case the only required parameters are M_0 and δ/h, where h is the step height or base height. The physical reasoning for these additional parameters in the axially-symmetric case can be explained by the effect of the streamline curvature as discussed by D.R. Chapman (Ref. 15). The axially-symmetric flow pattern results in the curving inwards of the external boundary separation region. This results in increasing the deflection of the streamlines towards the body's axis. Eventually this streamline slope may exceed the maximum angle of turning through a conical shock. In this case the recompression shock must be established at a point which is above the center line, resulting in an effective "center core". Attempts to correlate the pressure measurements available in References 6, 8, 15, 16, 18, 21 and 23 with a single parameter δ/h indicate a large scatter of the data and thus support the hypothesis that the additional parameters due to the axially-symmetric geometry must be included in order to correlate the data.

A. Experiments with "small diameter" models

Some measurements of pressure distribution behind axially-symmetric backward facing steps with turbulent flow separation were performed in this laboratory and were reported in Ref. 6. The model's forebody is a cone-cylinder. Few pressure holes are located ahead of the step while most are distributed behind the step. A typical pressure distribution is shown in Fig. 13. These measurements can be correlated by the parameter $h Re_L^{1/5}/L \approx h/\delta$, as shown in Fig. 14. This parameter is similar to the blunt nase correlating parameter rather than the two dimensional backward facing step one (which was found to be $h Re_L^{-3/5}/L$).

In these models $2h/D$ varied between 0.067 and 0.266. It is expected that as $2h/D \to 0$ the

axially symmetric backward facing step flow should become locally similar to the two dimensional one. The measurements of Ref. 6 indicate that in order to obtain this similarity the local radius of curvature must be very large, i.e. 2h/D very small.

B. Experiments with "large diameter" models

The axially symmetric separated flows cannot be treated by a simple modification of the two dimensional separated flows due to the difference in the interaction between the external inviscid flow and the viscous mixing region in the respective cases. While it is expected that as the ratio between step height to forebody radius decreases the flow should become locally similar to the two-dimensional flow, the required "smallness" of this parameter still remains to be established. Preliminary results discussed previously indicate that the required value of 2h/D for this case may be much smaller and anticipated in curent works.

Models are designed and built for measurement of the pressure distribution behind a backward facing step with 2h/D values varying between 1/50 to 1/200 (compared to about 1/4 to 1/16 in the "small diameter" models). The basic model configuration is a hollow cylinder 100 mm OD and 95 mm ID. The model details are shown in Fig. 15. About 4 mm behind the models' leading edge steps of 1 mm to 0.25 mm height are machined. Pressure holes are distributed behind the step as shown in Fig. 15. Four holes are placed 90° apart, 1 mm ahead of the step, in order to determine the flow alignment and the upstream pressure. The pressure lines are then connected to a Scanivalve* Model D, capable of monitoring 48 pressures. The Scanivalve is fitted with a Statham** strain gage pressure transducer and the pressures are recorded on a Brown-Honeywell strip-chart recorder. This arrangement enables measuring and recording of the 18 pressures within the 10 sec. of wind-tunnel running time. The tests are run at Mach 2.25 in the 12" × 12" supersonic blowdown wind-tunnel. The model installed in the wind-tunnel is shown in Fig. 16.

The measured step pressure can be fitted into the turbulent two dimensional step data. These measurements are indicated on Fig. 7. The slightly higher pressures recorded on the "large diameter" axially symmetric step may be due to the lower efective turbulent Reynolds number at the step caused by the short upstream body.

* Scanivalve Co., San Diego, Calif.
** Statham Co., Los Angeles, Calif.

V. MEASUREMENTS OF FLOW STRUCTURE IN THE TWO-DIMENSIONAL NEAR WAKE

The aerodynamic parameters in the supersonic near wake can be obtained by the measurement of the total pressure, static pressure and stagnation temperature profiles. The measurements are performed in the near wake behind a two dimensional wedge-flat plate model shown in Fig. 17.

1. TOTAL PRESSURE MEASUREMENTS

Total pressure profiles are measured at various distances behind the base up to a distance of about 4.5 base heights. The probe is a flattened tip stainless steel tubing 0.022" O.D., flattened at the probe tip to 0.002" height. The pressure is read on a strain gage pressure transducer and is recorded on the Y channel of a X – Y recorder. The probe position is monitored by a rectilinear carbon film potentiometer (manufactured by Computer Control Ltd.) with linearity of 0.5%, stroke of 2 inch and resolution of 1/35,000 inch. The position monitor is connected to the X channel of the X – Y recorder. A diagram of this system is included in Fig. 17. The total pressure profiles are measured along the tunnel center line and some profiles are measured about 1 inch off center in the lateral direction in order to check any spanwise variation in the flow profiles. Measured total profiles at Mach 3.5 are shown in Fig. 18. The various flow regimes of the near wake are clearly indicated in these measurements.

2. STATIC PRESSURE PROFILE

Static pressure measurement is sensitive to flow direction in respect to the probe as well as to disturbances due to the probe. The static pressure probe designed to standard specifications is shown in Fig. 17. Due to the probes' forebody, static pressures can be measured in the wake only from station 20 mm behind base. In the "dead air" region right behind the base the static pressure is indicated by the base pressure. Approximate static pressure value is also obtained by the total pressure probe measurements in the "dead air" region. These measurements indicate static pressure variation behind the base as shown in Fig. 19.

3. RECOVERY TEMPERATURE PROFILES

Total temperatures can be measured in supersonic flows with a calibrated shielded thermocouple probe (Ref. 29). The probe recovery factor is a function of both Mach and Reynolds numbers. The pre-

sent probe is designed with a view for miniaturization in order that it can be introduced into the near wake with minimum effects on the flow.

Two probe sizes are used. One is a 6 mm OD probe similar to E. Winkler's probe described in Ref. 30. A second probe with 3.0 mm OD has been built and used for most of the wake measurements. The probes are shown in Fig. 20. The probes use a glass radiation shield coated with bright platinium. The 3 mm probe has a teflon insert into which the iron-constant thermocouple leads are inserted. Vent holes are provided as shown in Fig. 20. The variation of the recovery factor of the probes is shown in Fig. 21.

The profiles of recovery temperature are then measured behind the blunt base in the traversing arrangement shown in Fig. 17. The recovery temperature profiles measured at Mach number 3.5 at various distances behind the blunt base are shown in Fig. 22.

The probe temperature measurements shown in Fig. 22 are most interesting. One can note that initially the probe temperature profile tends toward uniform distribution up to the "neck" position in the wake. Beyond this station various hot "jets" appear along the outside edges of the wake core.

These preliminary measurements are most interesting and further measurements are now planned. In order to obtain further details in the flow, miniature total temperature probes are being developed.

VI. SHOCK-TUNNEL DEVELOPMENT

1. The 10" × 12" Shock-Tunnel Description

The shock-tunnel is constructed by the modification of the existing 75 mm × 75 mm shock-tube which is described in Ref. 4. A convergent-divergent nozzle is added at the end of the low pressure section to enable the attainment of hypersonic Mach numbers. The shock-tunnel is constructed of the following sections: –

(a) **The Compression Chamber** is a 80 mm I.D. steel tube 2 meters long, capable of operating up to 3000 psi.

(b) **The Low Pressure Section** is a 75 mm × 75 mm cross section 7 meters long tube constructed of three 2 meters long sections and one 1 meter long section. The last three meters of the low pressure tube are instrumented with wall plugs for shock wave speed detection. Windows and mounting ports are

placed at station 6.8 meters and are used as the test section for shock tube operation.

(c) Hypersonic Nozzle is attached at the end of the low pressure tube. The convergent nozzle reduces the test section to a throat of 1.5 × 1.5 cm. The nozzle is then expanded by two stage expansions to section of 25 × 30 cm. A second diaphragm is provided between the low pressure tube and the nozzle enabling evacuation of the hypersonic nozzle section to few microns Hg. in order to facilitate the flow starting process in the hypersonic nozzle. A deflection plate turns the flow ahead of the main nozzle entrance by 10%. The nozzle design is shown in Fig. 23 and the tunnel is shown in Fig. 24.

2. Shock Tunnel and Shock Tube Instrumentation

a) Shock Speed Measurements. The shock speed is measured by the determination of the time of passage of the shock between two thin film gages mounted on the shock tube wall a known distance apart. The gages response is fed to the start and stop channels of a Berkley type 7360 1 mc counter.

b) Pressure Measurement. The pressure behind the reflected wave at the nozzle entrance, which corresponds to the shock-tunnel stagnation pressure, is measured by a type 14 Kistler transducer and recorded on one channel of Tektronix type 565 osciloscope. A sample pressure record is shown in Fig. 25.

c) Heat Transfer Measurements. One of the most important functions of shock-tube and hypersonic shock-tunnel instrumentation, is the measurement of heat transfer rates to the surface of models which are exposed to the high stagnation enthalpy flows.

This measurement can be accomplished by the use of thin film resistance thermometers, which consist of a thin metallic film deposited on an insulator substrate. The gages are then mounted flush with the surface of the model and take on the instantaneous local surface temperature.

The metallic film responds almost instantaneously (Ref. 31) to the time variations of the surface temperature of the substrate which is assumed to be, during the short duration of the test, approximately a semi-infinite, homogeneous, and isotropic, one-dimensional solid heat sink (Ref. 32). A constant low current is passed through the film resulting in a voltage signal across the gage. This signal is a function of the instantaneous resistance which is related to its temperature (this relation is linear for temperature changes less than 50°F). The voltage signal is then proportional to the surface temperature.

The heat flux history can be calculated from the measured time-temperature relation by solving the classical one dimensional heat conduction equation subject to the relevant boundary conditions.

The heat transfer rate $\dot{q}_0$ can now be calculated from the solution of the heat conduction equation if the calibration characteristics of the thin-film gage are known.

The simplest way to determine these gage characteristic parameters is to calibrate the gage by subjecting it to a known constant heat flux, record its output and calculate the calibration parameter of the gage from the one dimensional heat conduction theory.

The production of a sudden constant heat flux for such a calibration method is complicated by various errors introduced during this process.

A calibration circuit developed in this laboratory which subjects the film gage to a known sudden heat flux is described in Ref. 10. This calibration circuit has a very low noise level and satisfactory accuracy and repeatability.

The same calibration circuit is also used to calibrate a passive electrical analog network which is designed to convert the thin-film-gage surface temperature response into a signal which is a measure of the heat transfer rates (Ref. 33).

The application of the analog network replaces the calculation (using a digital computer) of the instantaneous heat transfer rates from the measured surface temperature histories. The accuracy of this method depends on the accuracy of the calibration of the analog network. The input signal into the network has to simulate exactly the thin-film gage output at a known heat transfer rate, which is not easy to achieve (Ref. 33). The present thin-film gage calibration circuit and its response characteristics, which are similar to the gage response in the shock tube application, enable a direct calibration of the analog network.

The heat transfer rate can then be evaluated by the relation (Ref. 10).

$$\dot{q}_0 = \{[\pi (\rho C k)_b^{1/2}]/(2 \alpha R_0 I_0)]\} (\Delta V/t^{1/2}) \tag{25}$$

The heat transfer rate $\dot{q}_0$ can be evaluated from Eq. (25) only if two physical parameters of the thin-film gage are known: These are the thermal resistivity α, and the thermal diffusivity parameter $(\rho C k)_b$.

The ratio $a/(\rho C k)_b^{1/2}$ can be determined directly by applying a known heat input to the gage and measuring the gage output. The calibration method suggested by Rabinowics (Rom) (Ref. 32) and Bogdan (Ref. 4) is based on the discharge of a large capacitor through the film. Difficulties experienced with the mercury relay switch used for initiating the discharge are found to be detrimental to the accuracy of this method.

A widely used method in shock-tube heat transfer research is the use of the bulk thermal diffusivity of the pyrex backing material $(\rho C k)_b = 0.067$ Btu/°F ft$^{1/2}$ sec$^{1/2}$, while the thermal resistivity is determined by the standard steady state technique. The use of bulk quantities for the deposited film has been always questioned. However, this method seemed to be acceptable considering the difficulties and inaccuracies encountered when more direct measurements of the calibration constants were tried.

The present method is based on electrical discharge of a known current into the film. The thin-film gage is placed into one arm of a carefully balanced wheatstone bridge. The bridge is balanced up to an unbalanced resistance of not more than 0.0005 ohms for a gage resistance of about 60 ohms. The imposed electric current is obtained from a constant voltage source and is applied to the gage through an electronic gate circuit which allows a constant voltage application for a 250 μsec. period. The circuit is shown in Figures 26 and 27. The signal and the electric current through the film are displayed on the Tektronix 565 dual beam oscilloscope. The oscilloscope is triggered 20 μsec. before the opening of the discharge gate circuit so that the zero voltage level is obtained for each discharge. The signal is displayed on the oscilloscope during a 200 μsec. period out of the available 250 μsec. gate time.

Using the circuit shown in Fig. 28, it is shown in Ref. 10, that the calibration constant is obtained by

$$\frac{a}{(\rho C k)_b^{1/2}} = \frac{4.1873\,\pi^{1/2}\,S}{2} \cdot \frac{R_0 + R_2}{R_2 R_0^2 I_0^3} \cdot \frac{E(t)}{t^{1/2}} \tag{26}$$

During the calibration run both $E(t)$ and $I(t)$ are recorded. When $E(t)$ is proportional to $t^{1/2}$ then $a/(\rho C k)_b^{1/2}$ is constant. The measured $E(t)$ is fitted by a parabolic time function by the use of the least mean square fit. This variation is then used to obtain the calibration constant from Eq. (26).

The data analysis procedure needed to evaluate the heat flux history from the temperature-time record is an expensive and time consuming process. An analog network is therefore devised following the example of Skinner (Ref. 33) which translates the surface temperature history into a flux history by solving the linear one-dimensional heat conduction equation in an approximate electric analog circuit. This circuit converts a voltage signal that is proportional to the instantaneous surface temperature into a voltage proportional to the heat flux.

Using the method proposed by Skinner (Ref. 33), a five section network is used as shown in Fig. 29. This network is tested with electrically pulsed thin-film gages and very satisfactory results are obtained with a noise level much lower than anticipated by Skinner (Ref. 33).

The analog network is now calibrated by the use of the output of a previously calibrated film. Using the calibration circuit, a known heat pulse can be applied to the gage. Feeding the gages' output through the analog network and recording the networks' output, results in a direct and simple procedure for this calibration.

The accuracy and repeatability of the calibration method are tested by repeated tests on various thin-film gages.

In order to ensure high accuracy the instantaneous current through the film must be carefully measured. The calibration constant $a/(\rho\, C\, k)_b^{1/2}$ depends on the third power of this current (Eq. 26). In the present circuit this current is measured, in each run, as a potential drop across a precision 1 ohm resistance and is recorded simultaneously with the film output (Fig. 30).

A different error source may be due to initial bridge unbalance. This unbalance will produce a step in output immediately upon application of the calibration discharge current. This initial step will shift the film calibration signal and must be accounted for during data reduction. In order to minimize this unbalance, all resistors used in the circuit are designed for high current capacity. The bridge is then balanced using a low D.C. current of 5 mA in order to minimize resistance changes (due to heating by the balancing current), while a high sensitivity galvanometer is used in order to obtain good balancing sensitivity. Despite the procedure a certain voltage jump is observed. A similar phenomena is also reported in Ref. 34. This initial jump can be correlated in the data reduction process by the computation of a best fit parabola. This fitted parabola defines a virtual zero point to its appex. It is found that about 30 μsec. after the trigger signal the shape of the gage output fits well the predicted parabolic

form. This "delay" is much longer than the electronic rise time of the system (which is measured to be about 4 μsec.). It may be due to the time required to establish one-dimensional heat flux during the calibration run. The overall calibration results, calculated by this method, are found to be within $\pm 1\%$ accuracy. This value is extremely good in comparison with other calibration techniques.

The output signal of the calibration circuit is used as an input signal for the calibration of the analog network which converts surface temperature history to heat transfer rate history. The film calibration output is a result of a constant heat rate pulse so that when it is fed to the analog network, it is expected that in this case the network output will be a step function. Due to the unexplained initial voltage jump in the film calibration output signal (discussed in the previous section) the input into the analog circuit is distorted. This distortion results in an initial overshoot of the analog network output, as seen in Fig. 31I. When the film calibration bridge is preset with a negative voltage bias, its output fits a parabolic rise almost instantaneously. When this signal is fed into the analog network its output indeed becomes a step function as seen in Fig. 31II. The signal to noise ratio for this analog network is approximately 20. The accuracy and repeatability are within less than $\pm 0.5\%$.

REFERENCES

1. Rom, J., Theory for supersonic two-dimensional laminar base type flows using the Crocco-Lees mixing concepts. Journal of Aerospace Sciences, Vol. 29, No. 8, August 1962. pp. 963 – 968.

2. Rom, J., and Victor, M., A theoretical and experimental determination of the base pressure behind a two-dimensional backward facing step in a laminar supersonic flow. Proceedings of the 5th Annual Conference on Aeronautics and Astronautics, Haifa, Israel. Jerusalem Academic Press. Feb. 1963.

3. Rom, J., and Seginer, A., Measurements of laminar heat transfer rates behind a two-dimensional backward facing step in the shock tube. Technical Note No. 6. Contract AF 61(052) – 576, TAE Report 25, March 1963.

4. Rom, J., Supersonic two-dimensional base type flow. Technical Report, Contract AF 61(052) – 576, TAE Report 27, March 1963.

5. Rom, J., Measurements of heat transfer rates in separated regions in a shock tube and in a shock tunnel. AIAA Journal, Vol. 1, No. 9, Sept. 1963, pp. 2193 – 2194.

6. Rom, J., and Victor, M., Base pressure behind two-dimensional and axially symmetric backward facing steps in a turbulent supersonic flow. Proceedings of the Sixth Israel Annual Conference on Aviation and Astronautics, Israel Journal of Technology, Vol. 2, No. 1, Feb. 1964, pp. 50 – 57.

7. Rom, J., and Seginer, A., Laminar heat transfer to a two-dimensional backward facing step from the high enthalpy supersonic flow in the shock tube – AIAA Journal, Vol. 2, Feb. 1964, pp. 251 – 255.

8. Rom, J., Supersonic flow over two-dimensional and axially-symmetric backward facing steps. Annual Summary Report No. 2, Contract AF 61(052)–576, TAE Report 33, March 1964.

9. Rom, J., Analysis of the near wake pressure in supersonic flow using the momentum integral method. Interim Scientific Report No. 5. Contract AF 61(052) – 576. TAE Report No. 35, Sept. 1964.

10. Seginer, A., Cohen, A., and Rom, J., – Calibration of thin film resistance thermometer for heat

flux measurements in the shock tube. Proceedings of the Seventh Annual Conference on Aviation and Astronautics, Israel Journal of Technology, Vol. 3, No. 1, Feb. 1965.

11. Crocco, L., and Lees, L., A mixing theory for the interaction between dissipative flows and nearly isentropic streams. Journal of Aeronautical Sciences, Vol. 19, No. 10, October 1952, pp. 649 – 679.

12. Glick, H.S., Modified Crocco-Lees mixing theory for supersonic separated and reattaching flows. GALCIT Hypersonic Research Project Memorandum No. 53, May 1960. Also, Journal of Aerospace Sciences, Vol. 29, No. 10, October 1962, pp. 1238 – 1244.

13. Korst, H.H., Page, R.H., and Childs, M.E. A theory for base pressure in transonic and supersonic flow. University of Illinois, ME TN – 392 – 2, OSR TN 55 – 89, March 1955.

14. Korst, H.H., Chow, W.L., and Zumwalt, G.W., Research on transonic and supersonic flow of a real fluid at abrupt increase in cross section. University of Illinois, Mech. Eng. Dept., M.E. Tech. Rep. 392 – 5 (AFOSR TR 60 – 74), December 1959.

15. Chapman, D.R., An analysis of base pressure at supersonic velocities and comparison with experiments. NACA TR 1051, 1951.

16. Chapman, D.R., Kuehn, D.M., and Larson, H.K., Investigation of separated flows in supersonic and subsonic streams with emphasis on effect of transition. NACA Rep. 1356, 1958.

17. Chapman, D.R., Wimbrow, W.R., and Kester, R.H., Experimental investigation of base pressure on blunt trailing edge wings at supersonic velocities. NACA Rep. 1109, 1952.

18. Gadd, G.E., Holder, D.W., and Regan, J.D., Base Pressure in supersonic flows. ARC 17490, C.P. 271, 1956.

19. Charwat, A.F., and Yakura, J.K., An investigation of two-dimensional base pressures. Journal of Aeronautical Sciences, Vol. 25, February 1958, p. 122.

20. Beheim, M.A., Flow in the base region of axisymmetric and two-dimensional configurations. NASA TR R – 77, 1961.

21. Dewey, C.F., Jr., The near-wake of a blunt body at hypersonic speeds. AIAA Preprint No. 64 – 43, January 1964.

22. Fuller, L., and Reid, J., Experiments on two-dimensional base flow at M = 2.4. ARC 18723, R & M 3064, 1956.

23. Roshko, A., and Thomke, G.J., Flow separation and reattachment behind a downstream facing step. Douglas Report SM–43056–1, January 1964.

24. Nash, J.F., An analysis of two-dimensional turbulent base flow including the effect of the approaching boundary layer. ARC R & M 3344, 1963.

25. Denison, M.R., and Baum, E., Compressible free shear layer with finite initial thickness. AIAA Journal, Vol. 1, 1963, pp. 342 – 349.

26. Kabota, T., and Dewey, F.C., Momentum integral methods for the laminar free shear layer. AIAA Journal, Vol. 2, 1964, pp. 624 – 629.

27. Goldstein, S., ed., Modern developments in fluid dynamics. Oxford University Press, 1938, pp. 131 – 134.

28. Lees, L., and Reeves, B.L., Supersonic separated and reattaching laminar flow: I. General theory and application to adiabatic boundary layer – shock wave interaction. GALCIT Technical Report No. 3, October 1963.

29. Landenburg, R.W., ed. Physical measurements in gas dynamics and combustion. High speed aerodynamics and jet propulsion, Volume IX. Princeton University Press, 1954.

30. Winkler, E.M., Design and calibration of stagnation temperature probes for use at high supersonic speeds and elevated temperatures. Journal of App. Physics Vol. 25, No. 2, Feb. 1954, pp. 231 – 232.

31. Hall, J.G., and Hertzberg, A., Advances in transient surface temperature thermometry, Jet Propulsion, Vol. 28, No. 11, Nov. 1958.

32. Rabinowicz, J., Jessey, M.E., and Bartschi G.A., Resistance thermometers for heat transfer measurements in a shock tube. GALCIT Hypersonic Research Project, Memo No. 33, July 1956.

33. Skinner, G.T., Analog network to convert surface temperature to heat flux. Rep. No. CAL – 100. Cornell Aero Lab. 1960.

34. Bogdan, L., High-temperature, thin-film resistance thermometers for heat transfer measurements, NASA CR – 26, Apr. 1964.

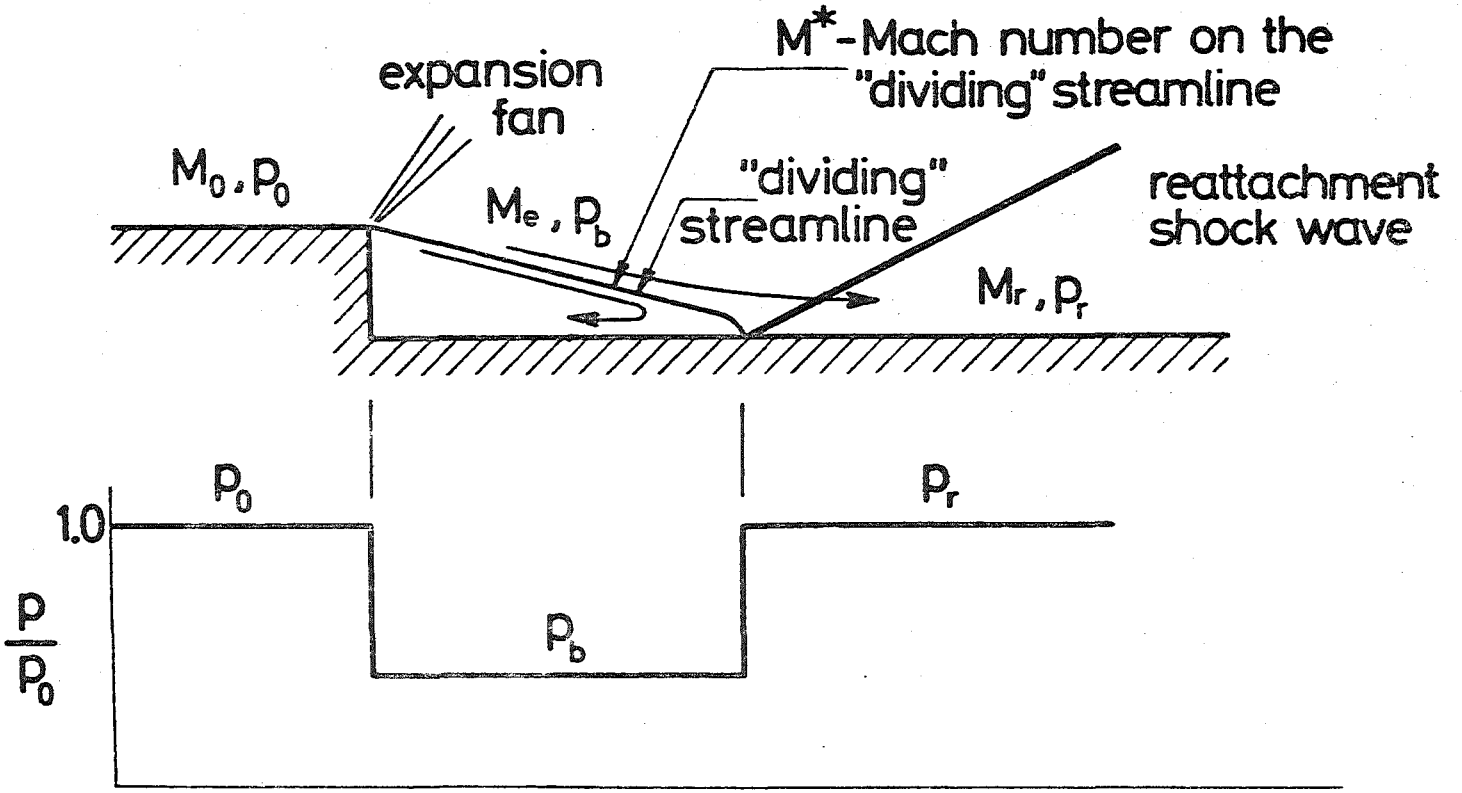

FIG. 1 THE KORST-CHAPMAN MODEL FOR SUPERSONIC FLOW OVER A BACKWARD FACING STEP

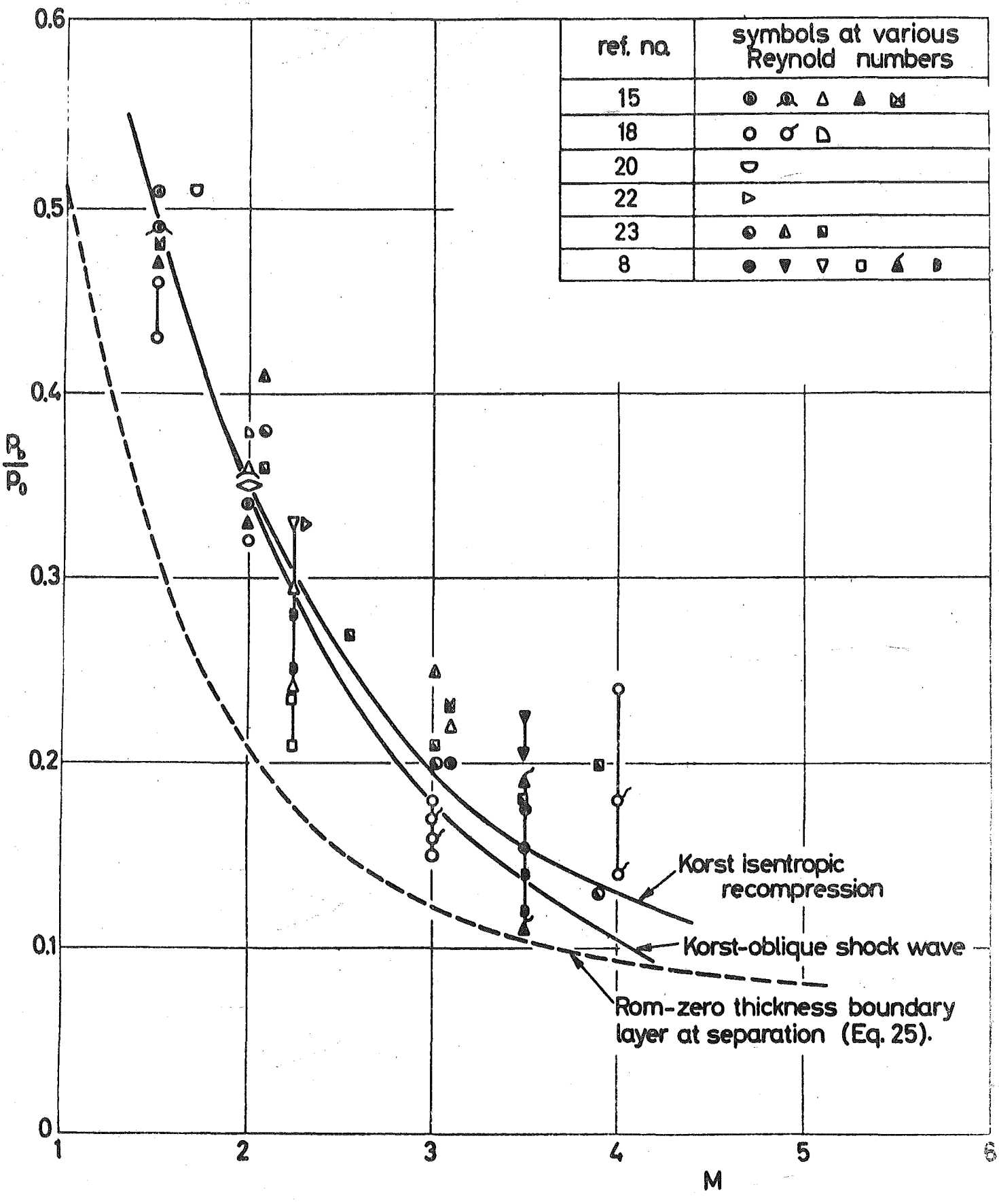

FIG. 2 THE BASE PRESSURE BEHIND A TWO DIMENSIONAL BACKWARD FACING STEP -TURBULENT SEPARATION

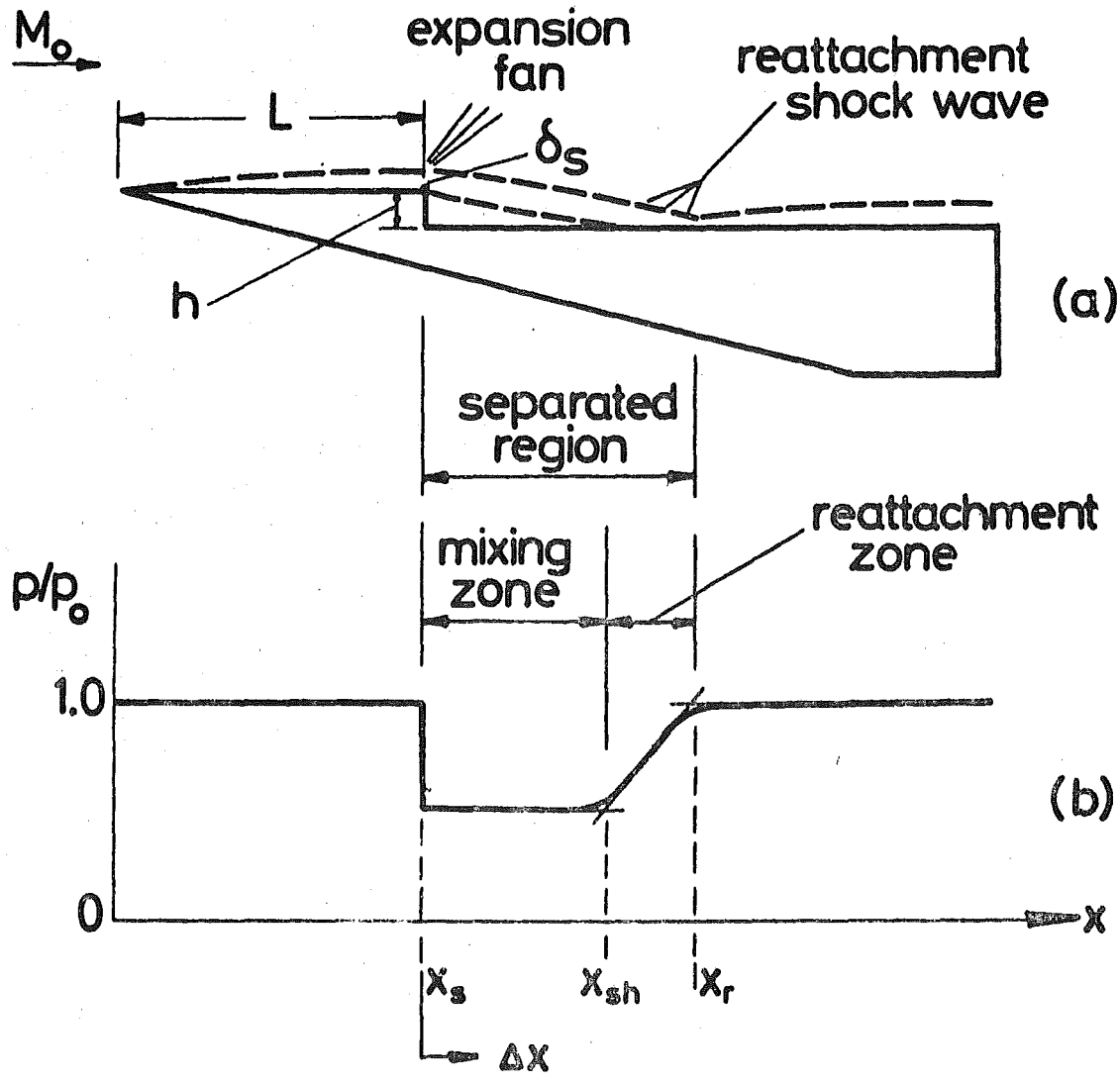

FIG. 3 SUPERSONIC FLOW OVER A BACKWARD FACING STEP

(a) physical flow field

(b) schematic pressure distribution

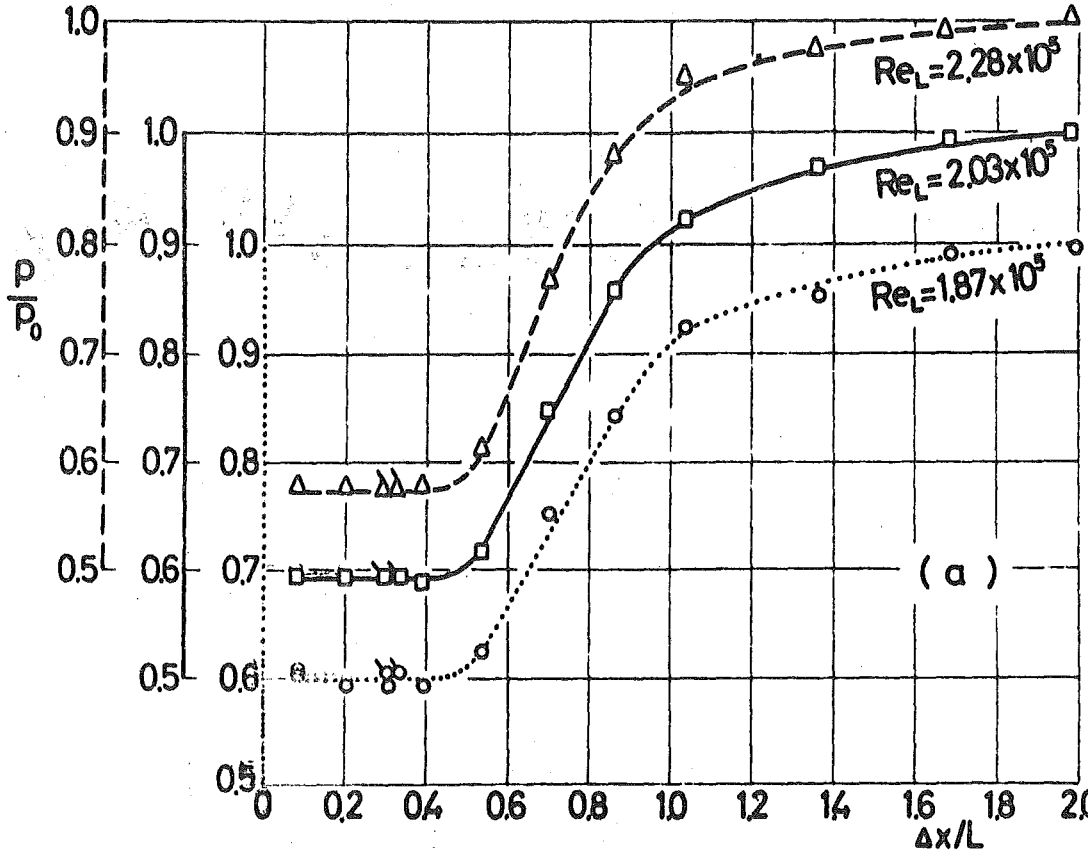

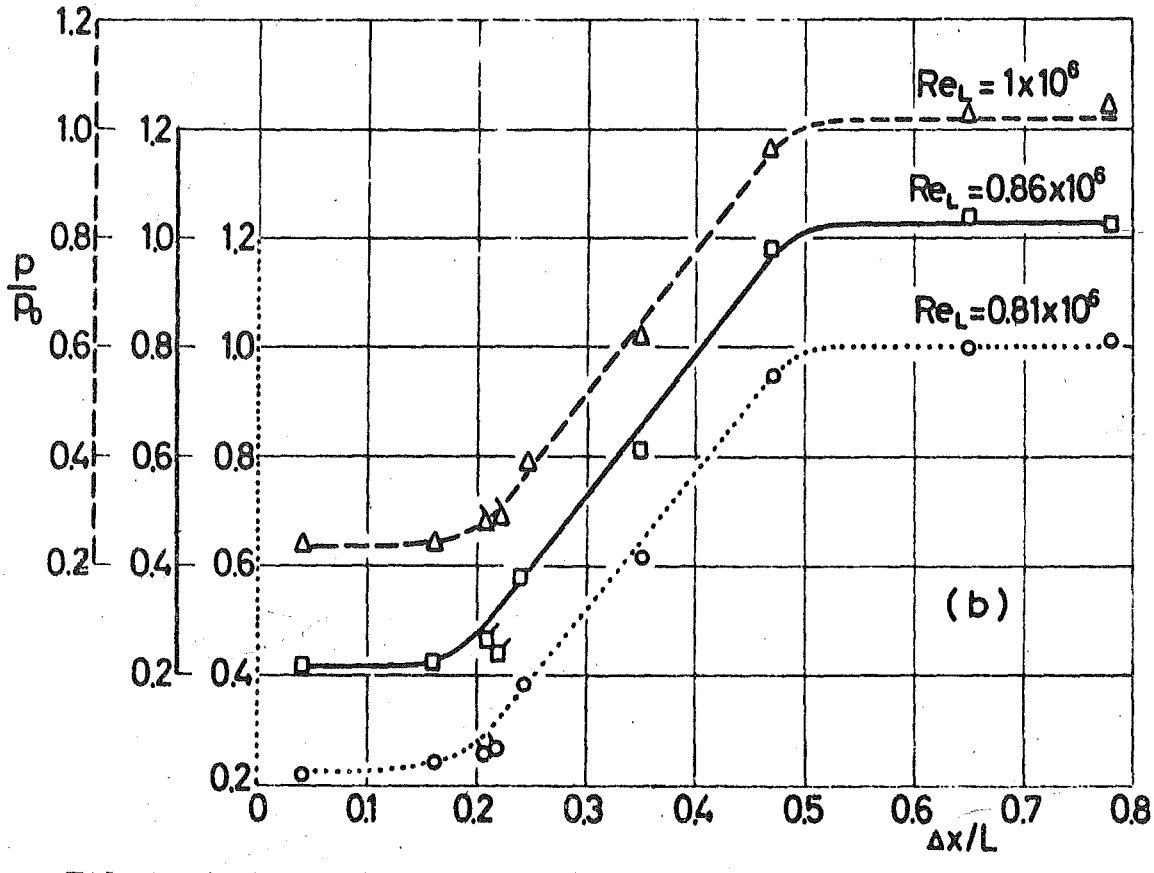

FIG. 4 TYPICAL PRESSURE DISTRIBUTIONS MEASURED OVER THE BACKWARD FACING STEP
(a) laminar flow (b) turbulent flow

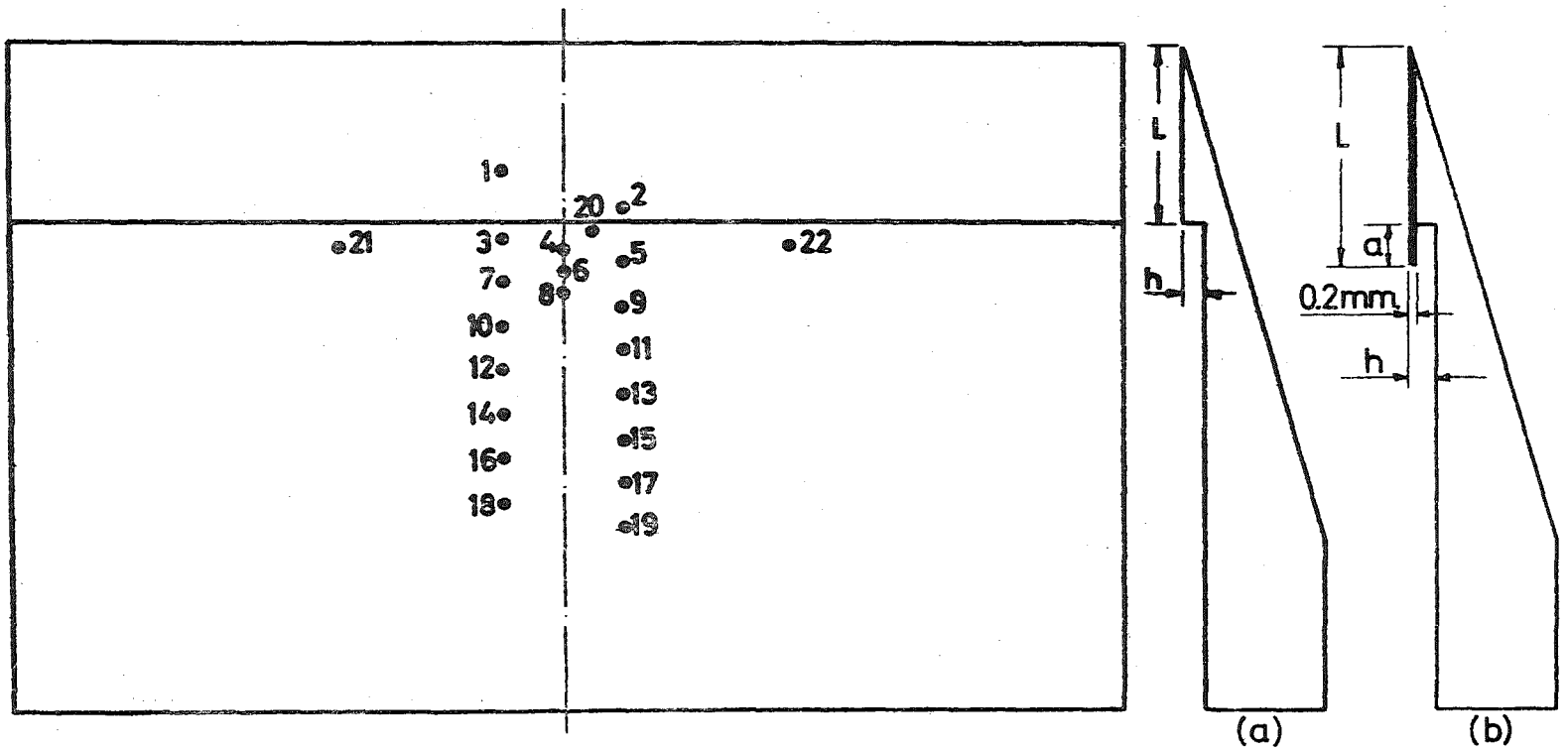

FIG. 5 BACKWARD-FACING STEP MODELS WITH PRESSURE HOLES LOCATION

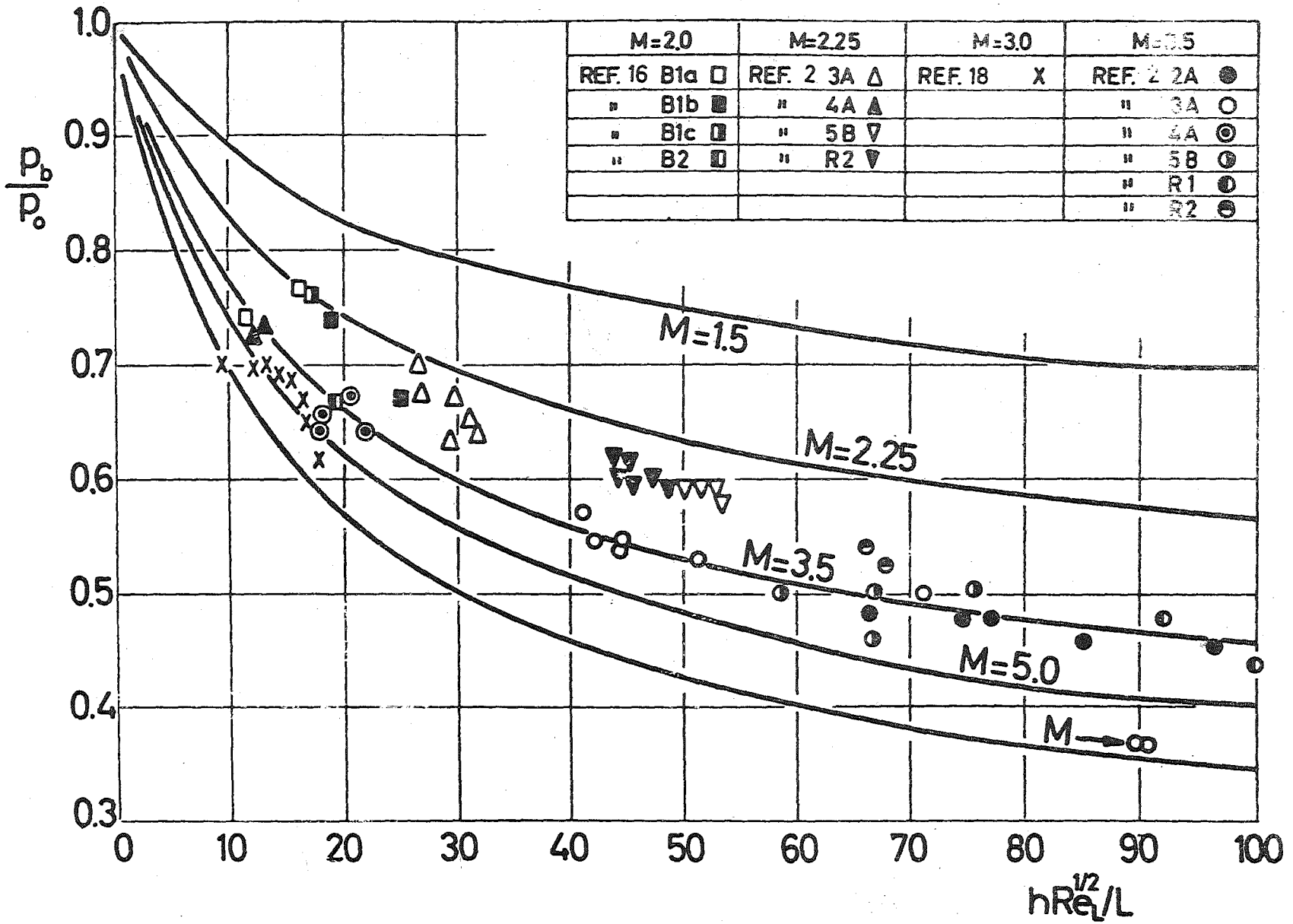

FIG. 6 LAMINAR BACKWARD FACING STEP BASE PRESSURE AS A FUNCTION OF $hRe_L^{1/2}/L$

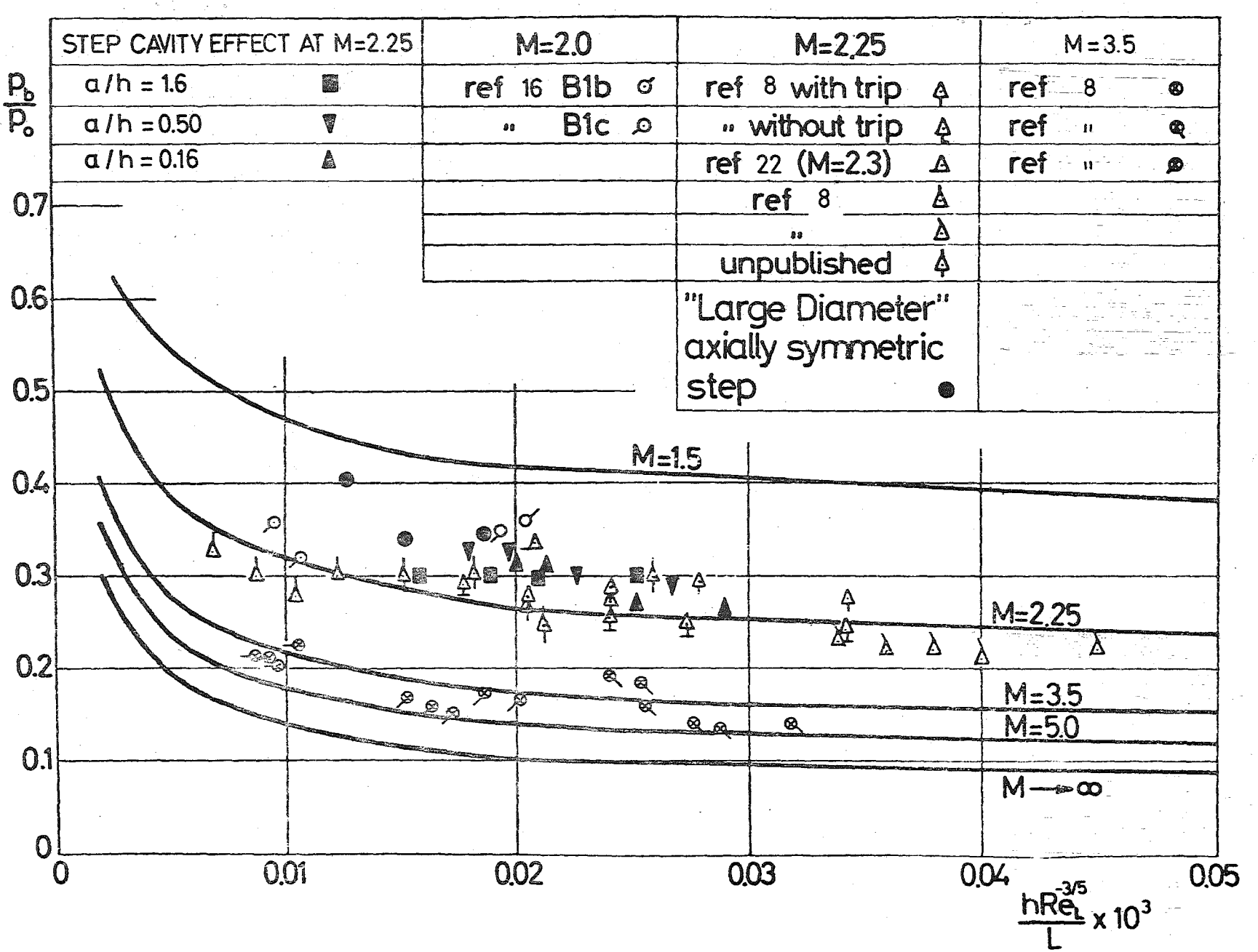

FIG. 7 THE TWO DIMENSIONAL BACKWARD FACING STEP PRESSURE p_b/p_o AS A FUNCTION OF $hRe_L^{-3/5}/L$ – TURBULENT FLOWS

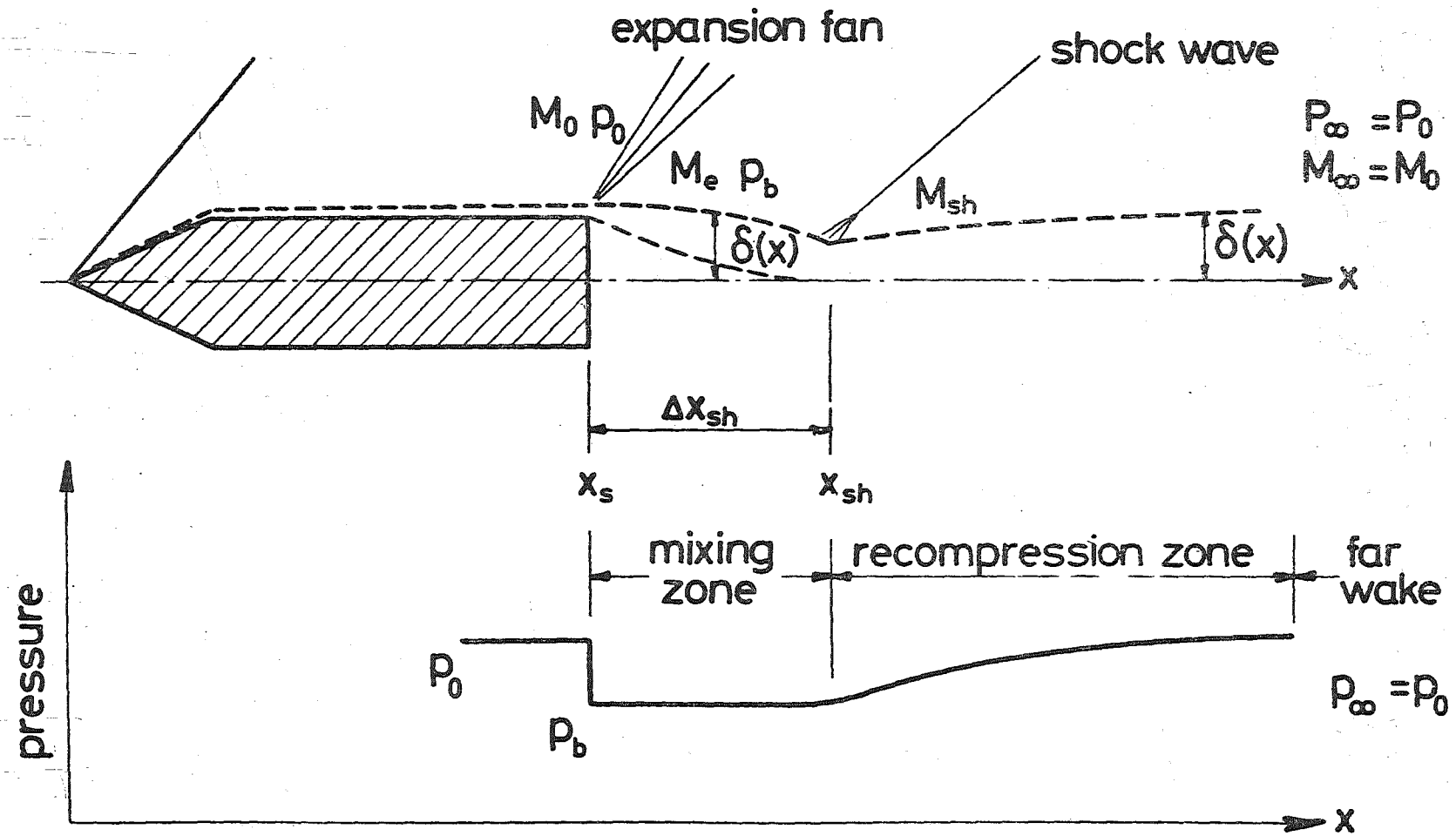

FIG. 8 SUPERSONIC FLOW OVER A TWO DIMENSIONAL BASE

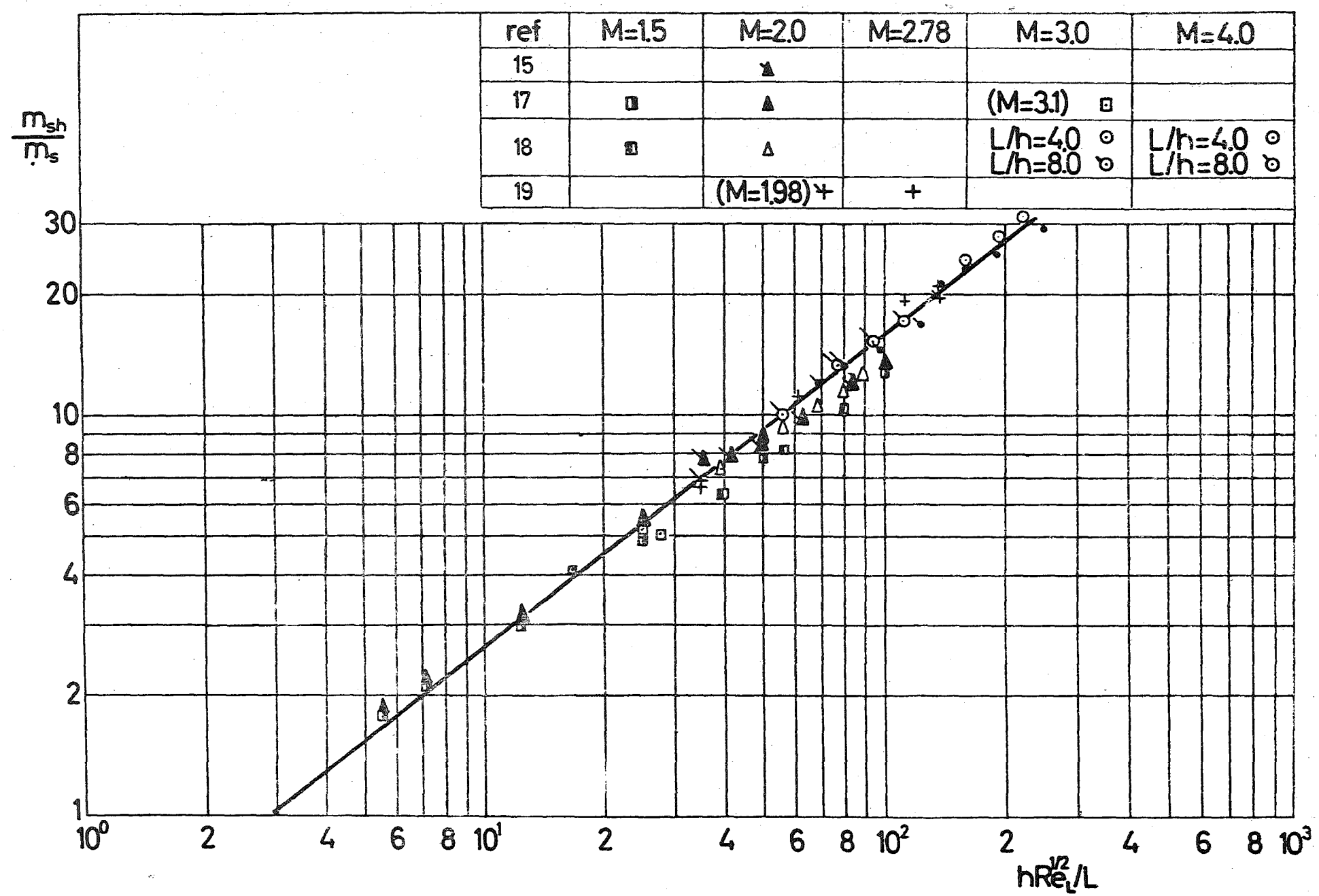

FIG. 9 THE LAMINAR MASS ADDITION m_{sh}/m_s AS A FUNCTION OF $hRe_L^{1/2}/L$ FOR TWO DIMENSIONAL BASE FLOW

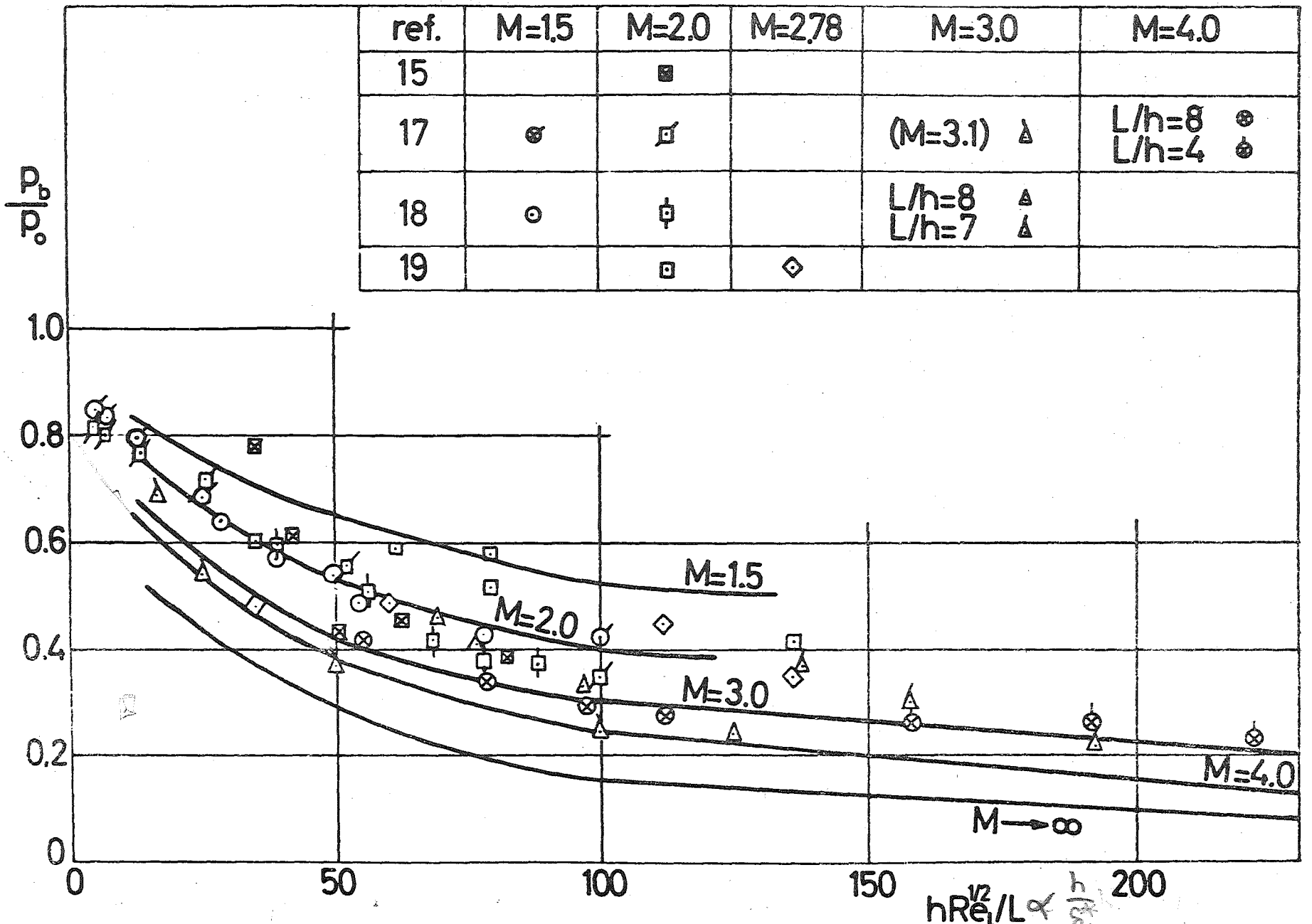

FIG. 10 TWO DIMENSIONAL BASE PRESSURE - LAMINAR FLOWS

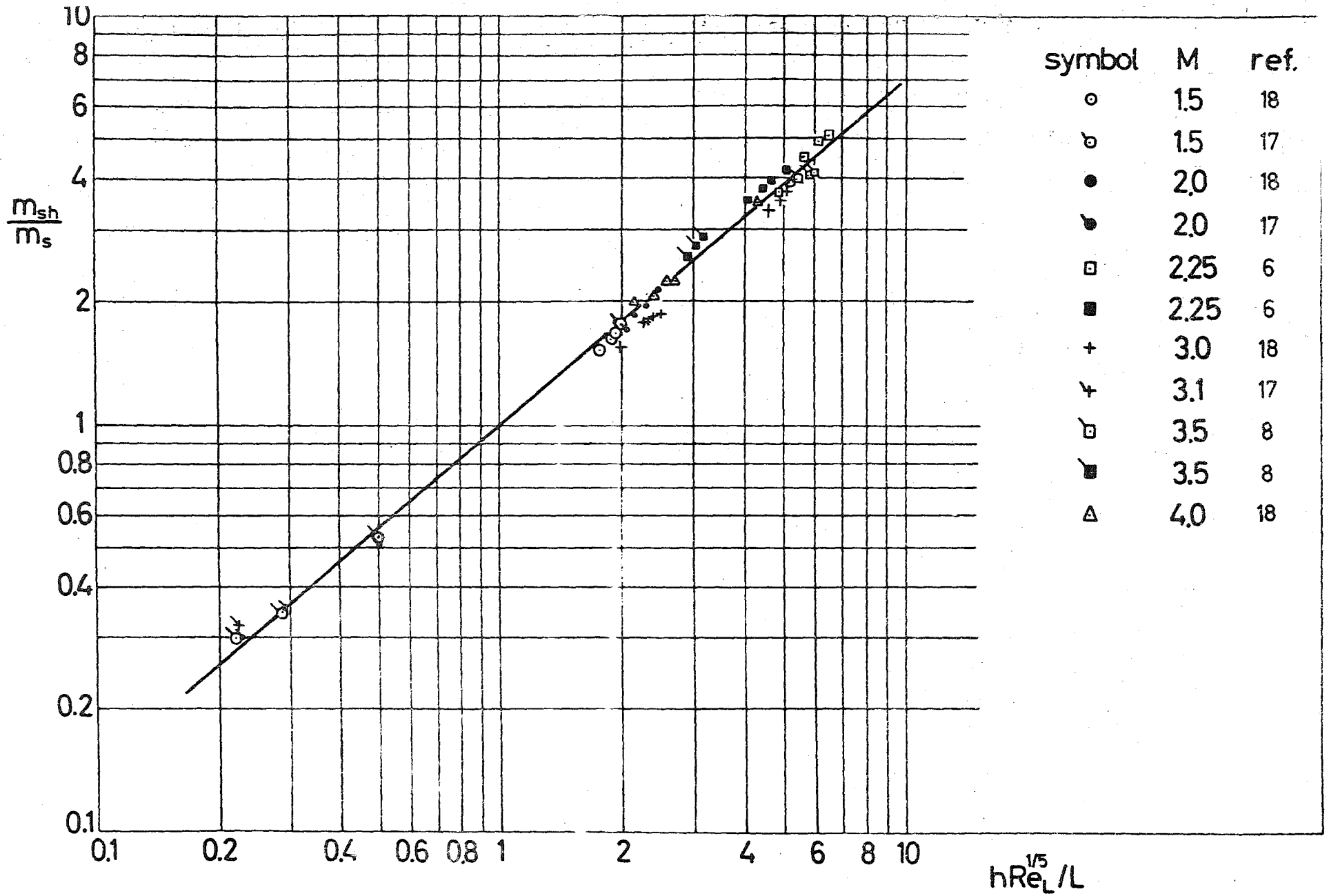

FIG. 11 THE TURBULENT MASS ADDITION m_{sh}/m_s AS A FUNCTION OF $hRe_L^{1/5}/L$ FOR A TWO DIMENSIONAL BASE FLOW

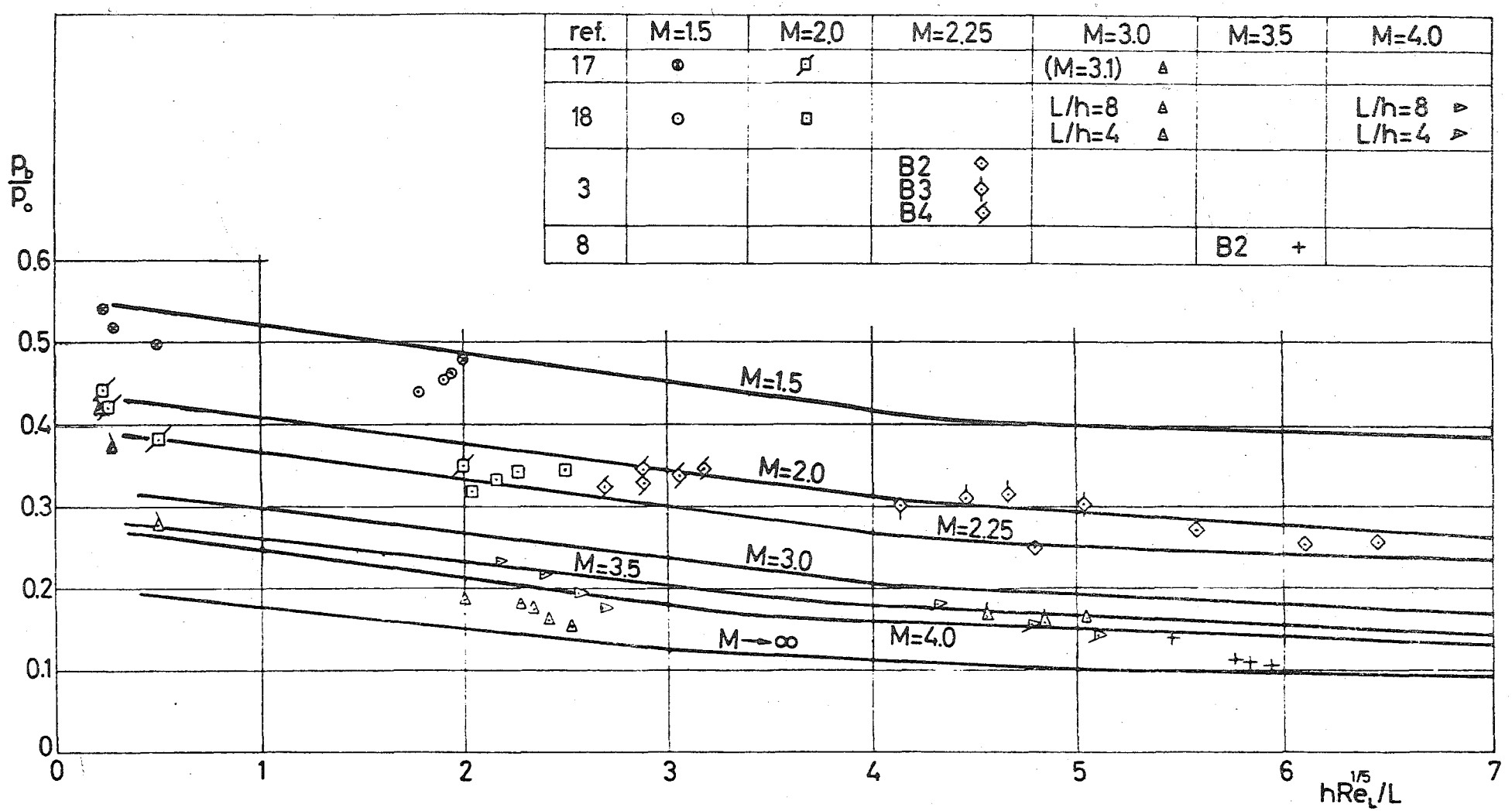

FIG. 12 TWO DIMENSIONAL BASE PRESSURE - TURBULENT FLOWS

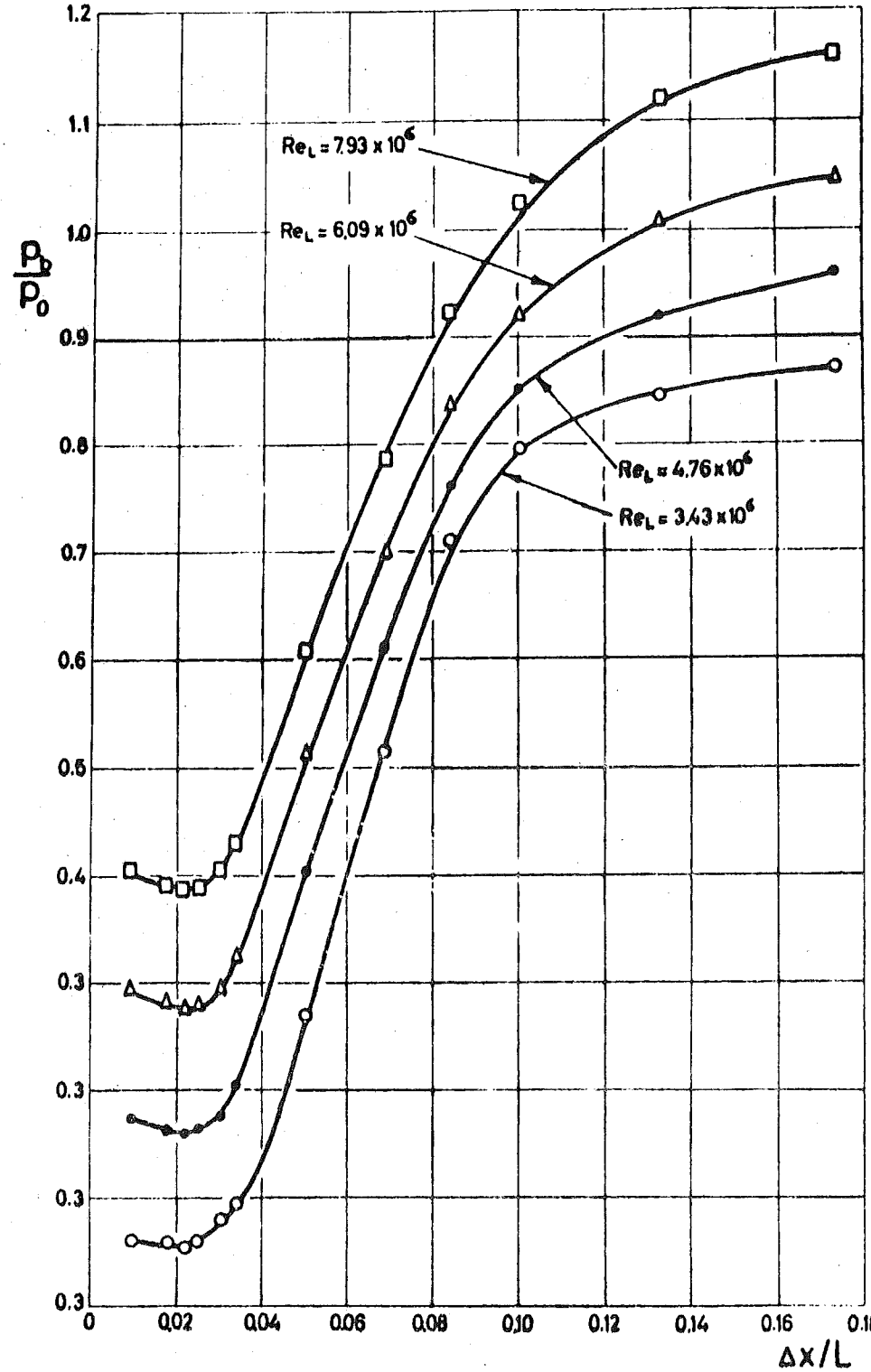

FIG. 13 PRESSURE DISTRIBUTION OVER AN AXIALLY SYMMETRIC BACKWARD FACING STEP OF L/h = 50.8 AT M= 2.25 AND VARIOUS REYNOLDS NUMBERS - TURBULENT FLOWS

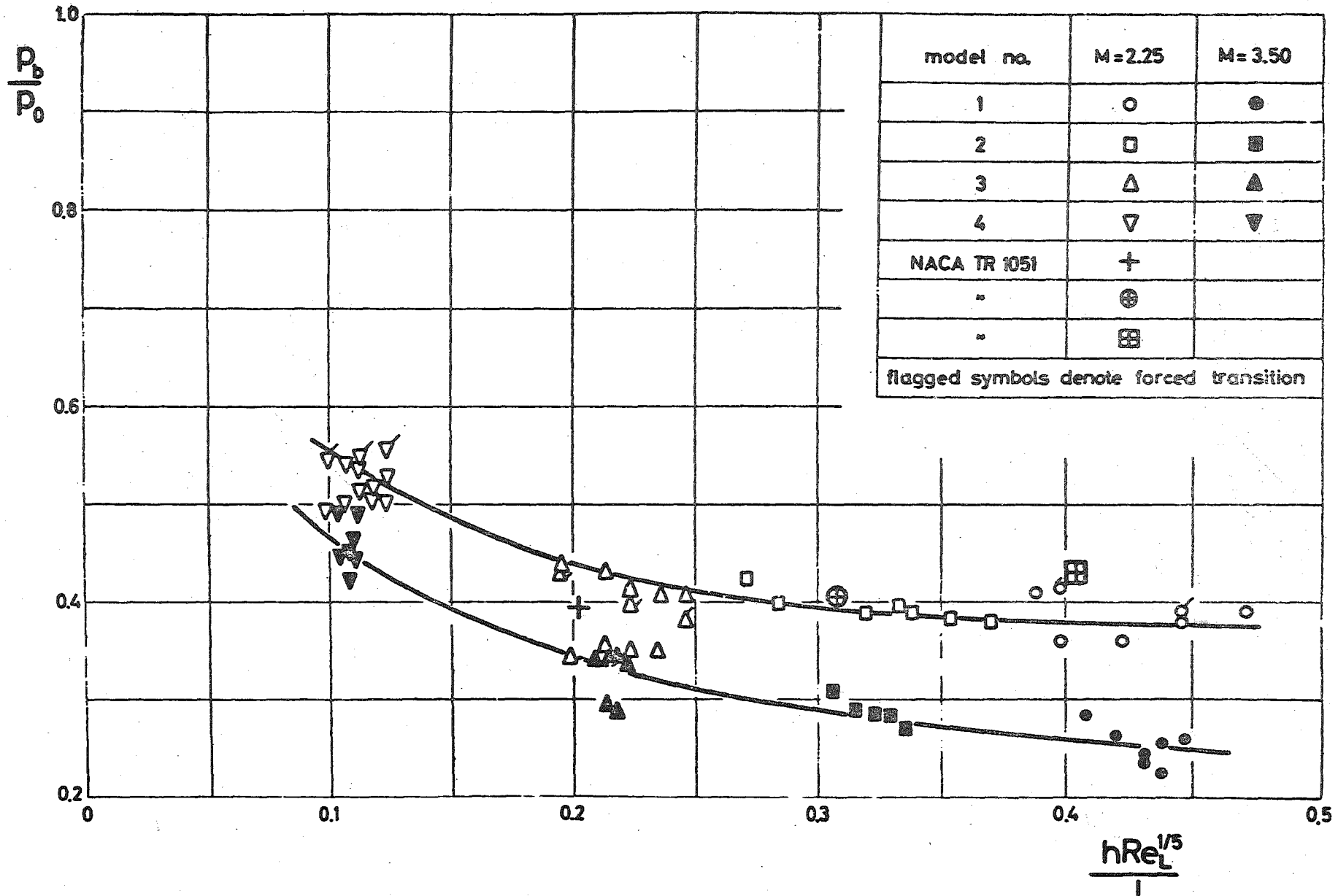

FIG. 14 THE AXIALLY SYMMETRIC BACKWARD FACING STEP PRESSURE p_b/p_0 AS FUNCTION OF $hRe_L^{1/5}/L$ - TURBULENT FLOWS

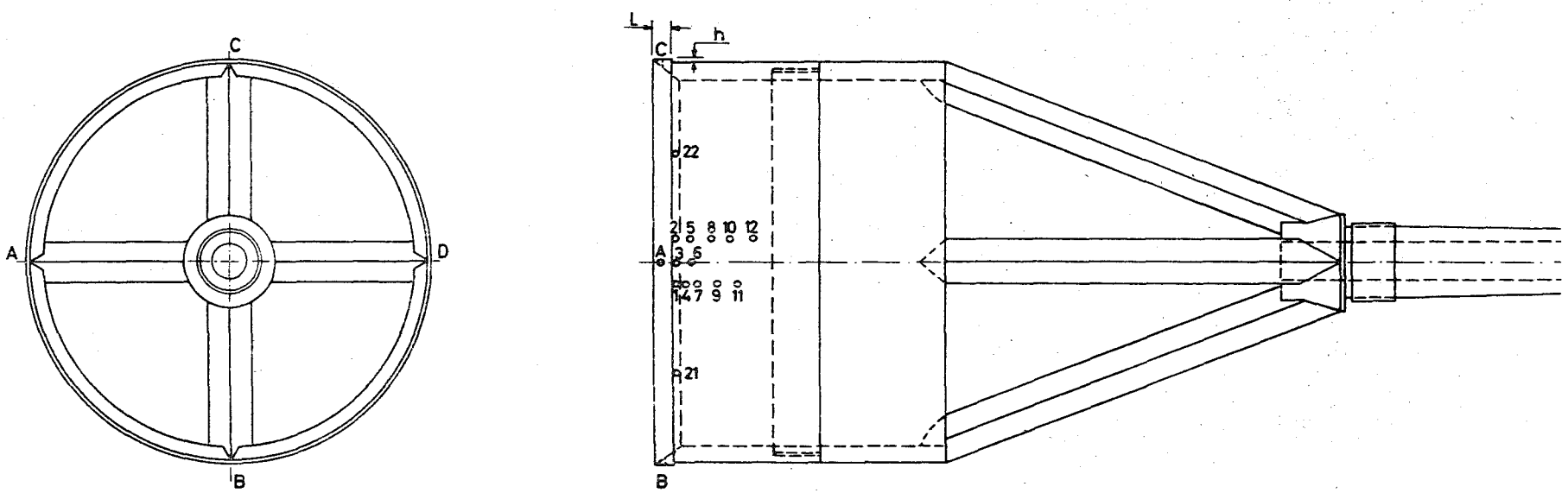

FIG. 15 THE LARGE DIAMETER AXIALLY SYMMETRIC BACKWARD FACING STEP MODEL

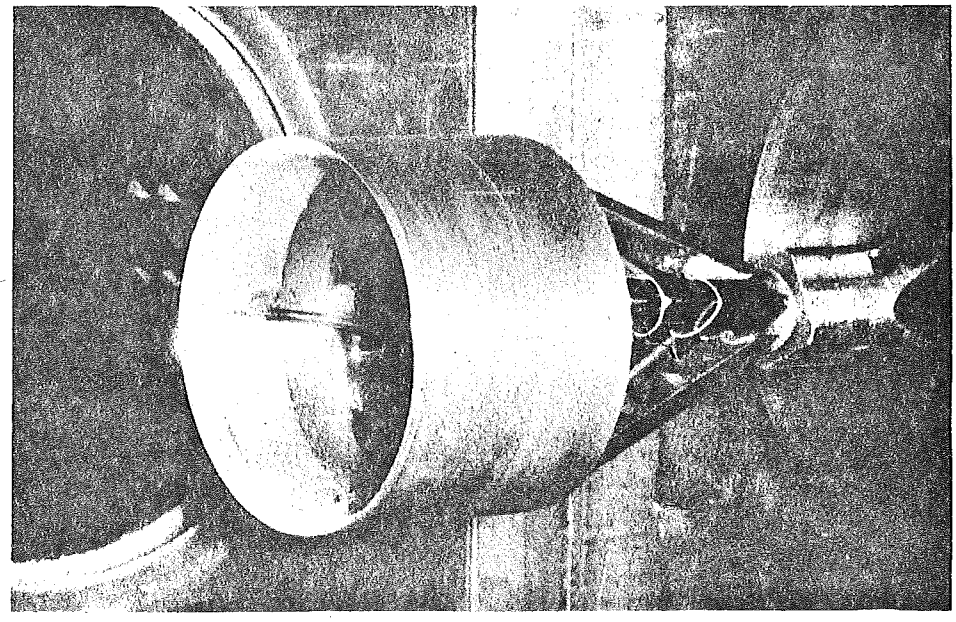

FIG. 16 THE LARGE DIAMETER MODEL INSTALLED IN THE 12"x12" WIND TUNNEL.

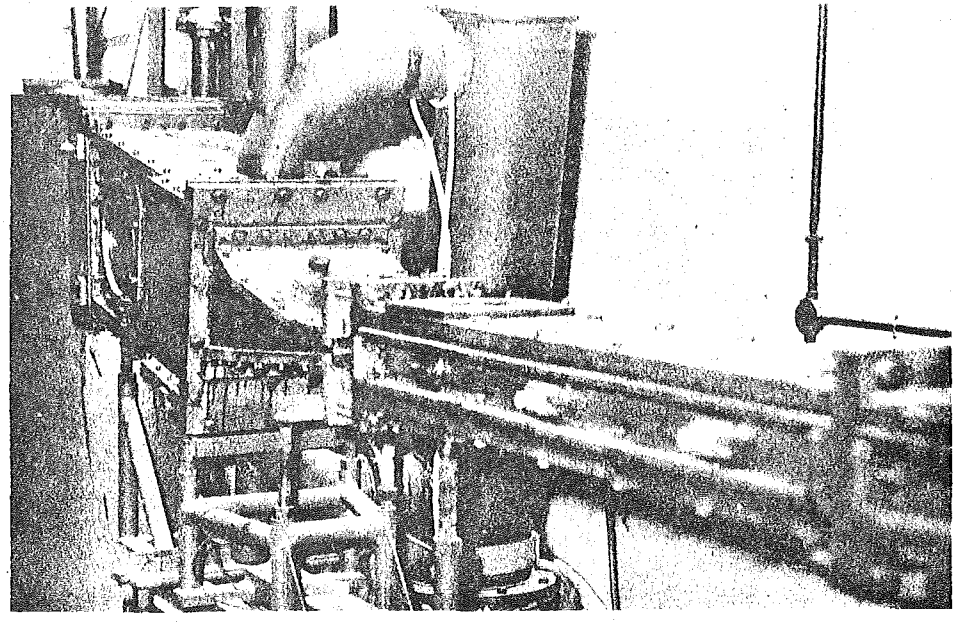

FIG. 24 THE 10"x12" HYPERSONIC SHOCK TUNNEL

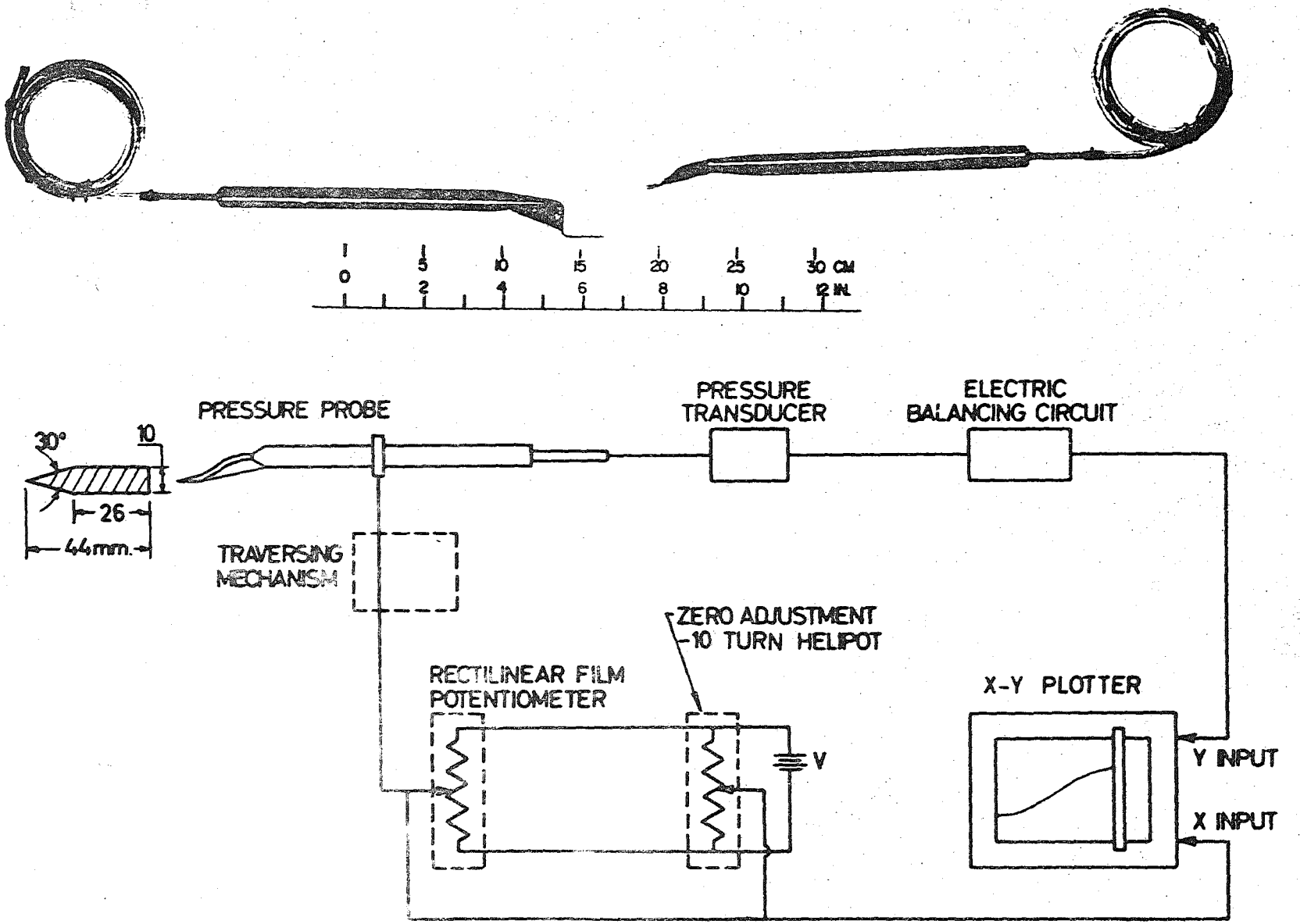

FIG. 17 SYSTEM FOR MEASURING AND RECORDING PRESSURE AND TEMPERATURE TRAVERSES IN THE BLOW DOWN WIND-TUNNEL IN THE NEAR WAKE OF A WEDGE FLAT-PLATE MODEL

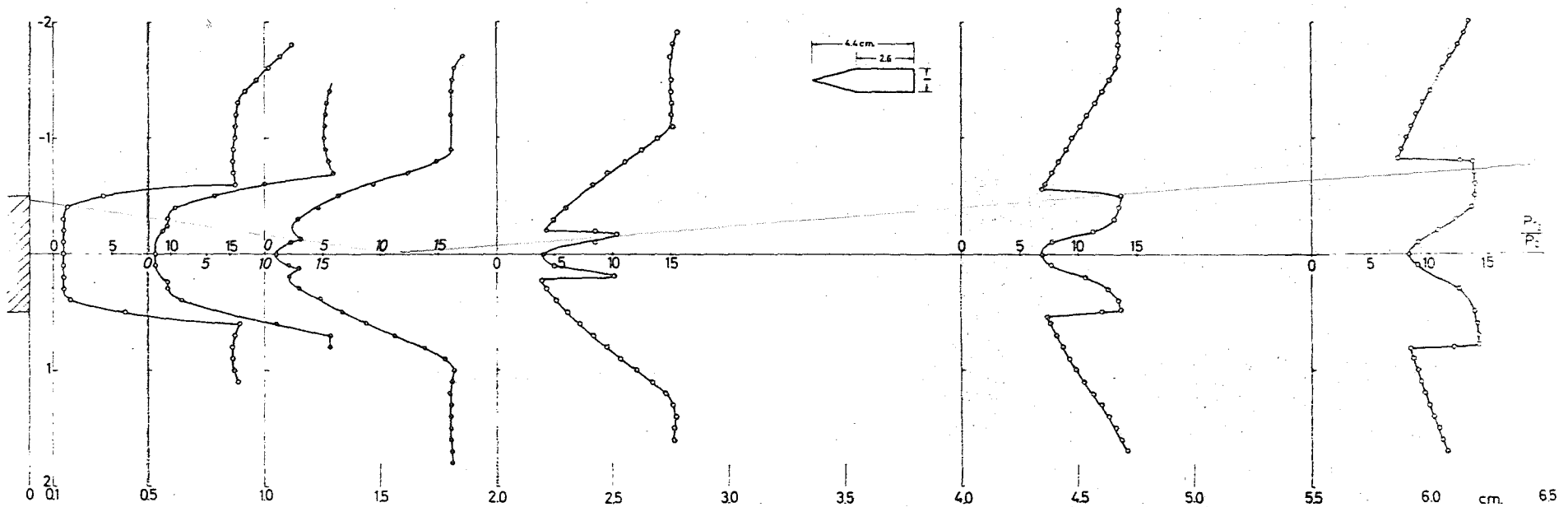

FIG. 18 TOTAL PRESSURE PROFILES IN THE TURBULENT NEAR WAKE BEHIND A BLUNT TWO DIMENSIONAL BASE AT M = 3.5

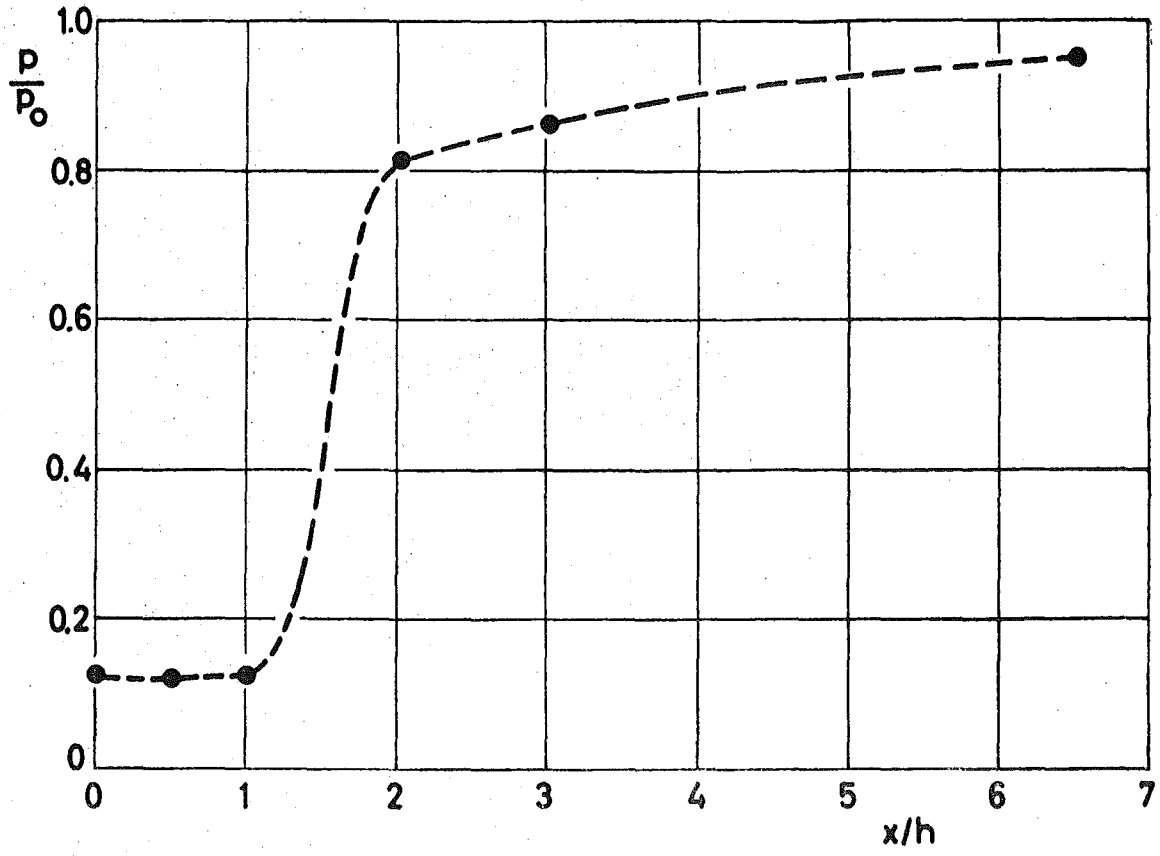

FIG. 19 STATIC PRESSURE VARIATION ALONG THE AXIS OF THE TURBULENT NEAR WAKE M=3.5

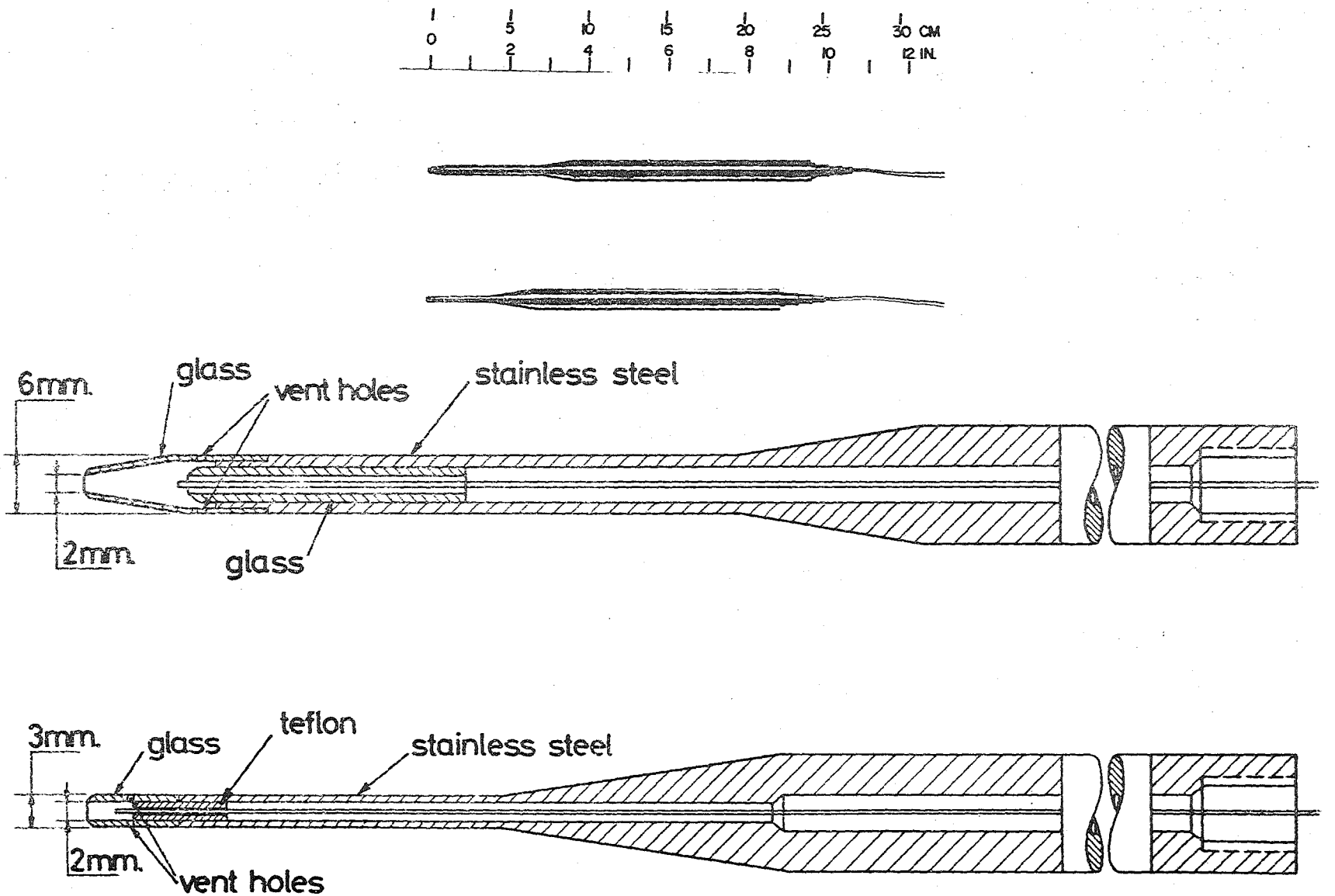

FIG. 20 TOTAL TEMPERATURE PROBES

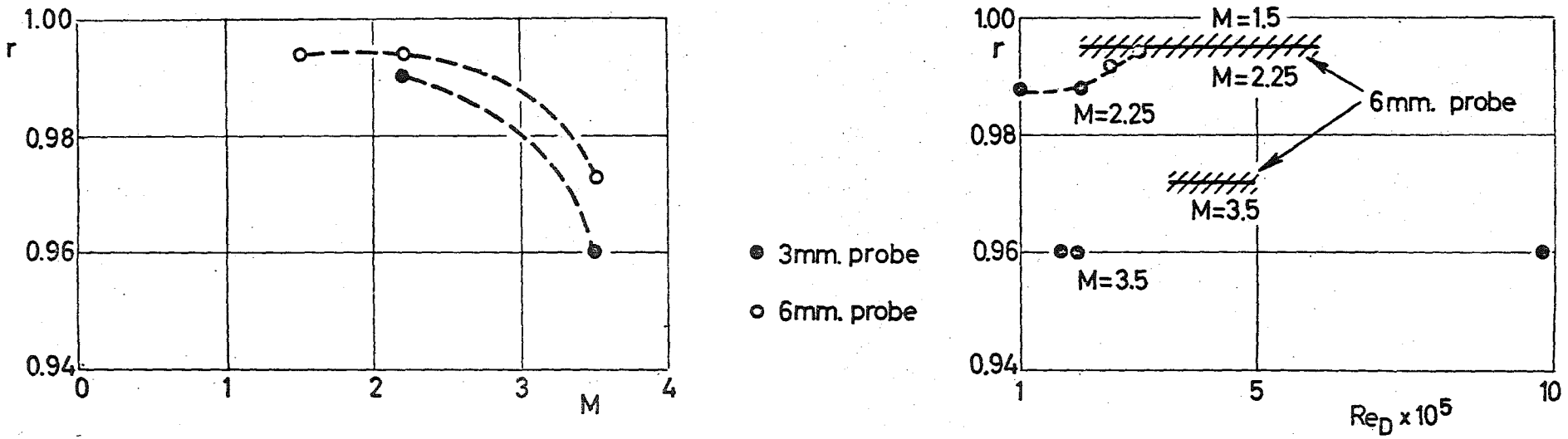

(a) VARIATION OF RECOVERY FACTOR WITH MACH NUMBER

(b) VARIATION OF RECOVERY FACTOR WITH REYNOLDS NUMBER

FIG. 21 RECOVERY FACTOR VARIATION FOR THE 3mm. AND THE 6mm. TOTAL TEMPERATURE PROBES

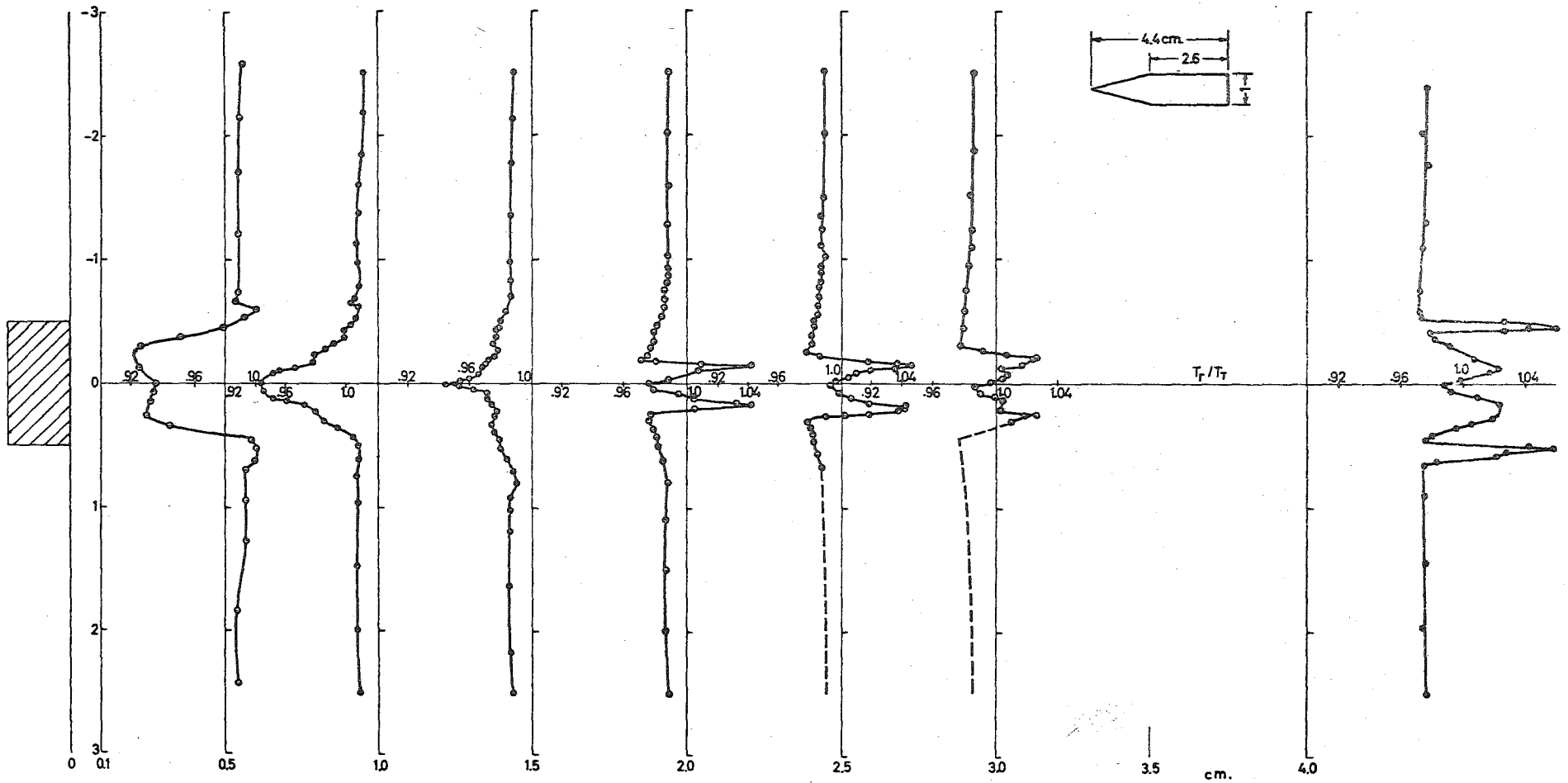

FIG. 22 RECOVERY TEMPERATURE PROFILES IN THE TURBULENT NEAR WAKE BEHIND A BLUNT TWO DIMENSIONAL BASE AT M=3.5

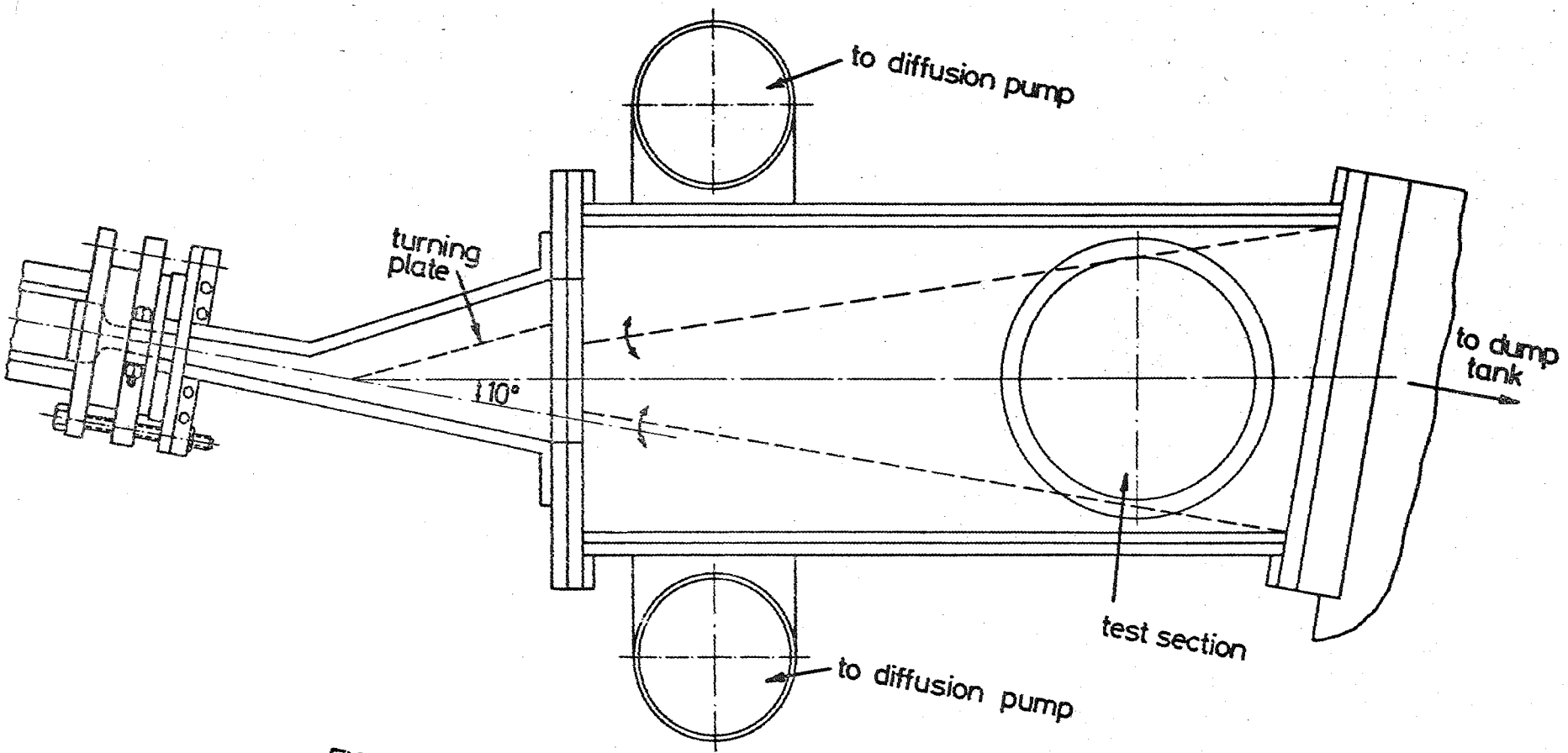

FIG. 23 THE HYPERSONIC SHOCK TUNNEL NOZZLE

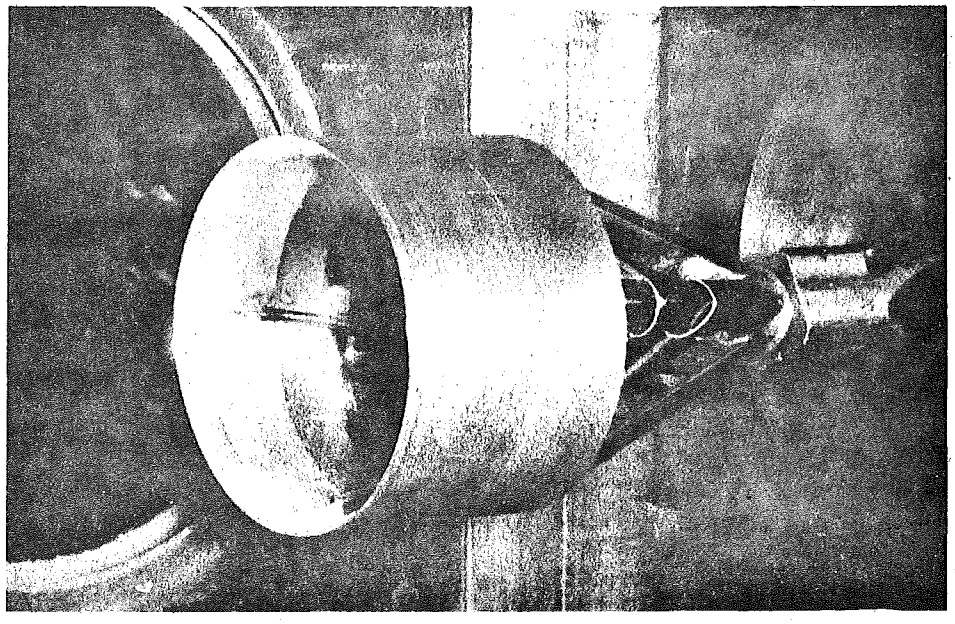

FIG. 16 THE LARGE DIAMETER MODEL INSTALLED IN THE 12"x12" WIND TUNNEL.

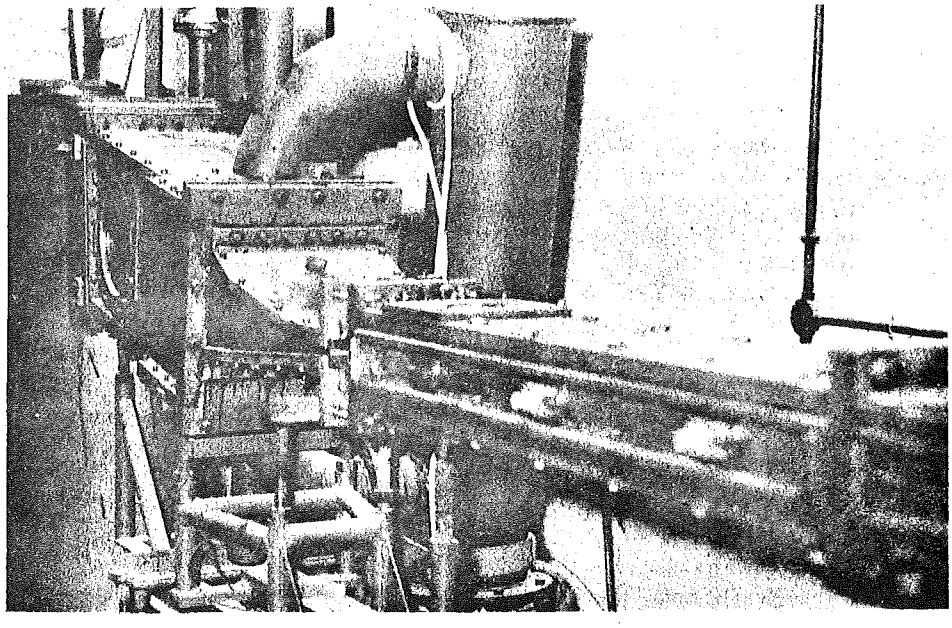

FIG. 24 THE 10"x12" HYPERSONIC SHOCK TUNNEL

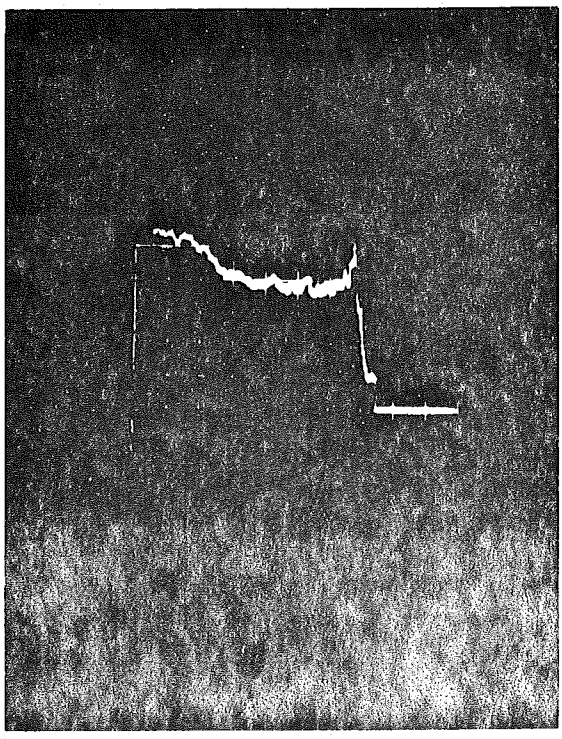

$M_s = 3$ $p_1 = 20$ mm Hg

SENSITIVITY : 0.4 VOLT / DIV.

SWEEP : 0.2 MSEC./DIV .

FIG. 25 SHOCK TUNNEL STAGNATION PRESSURE RECORD

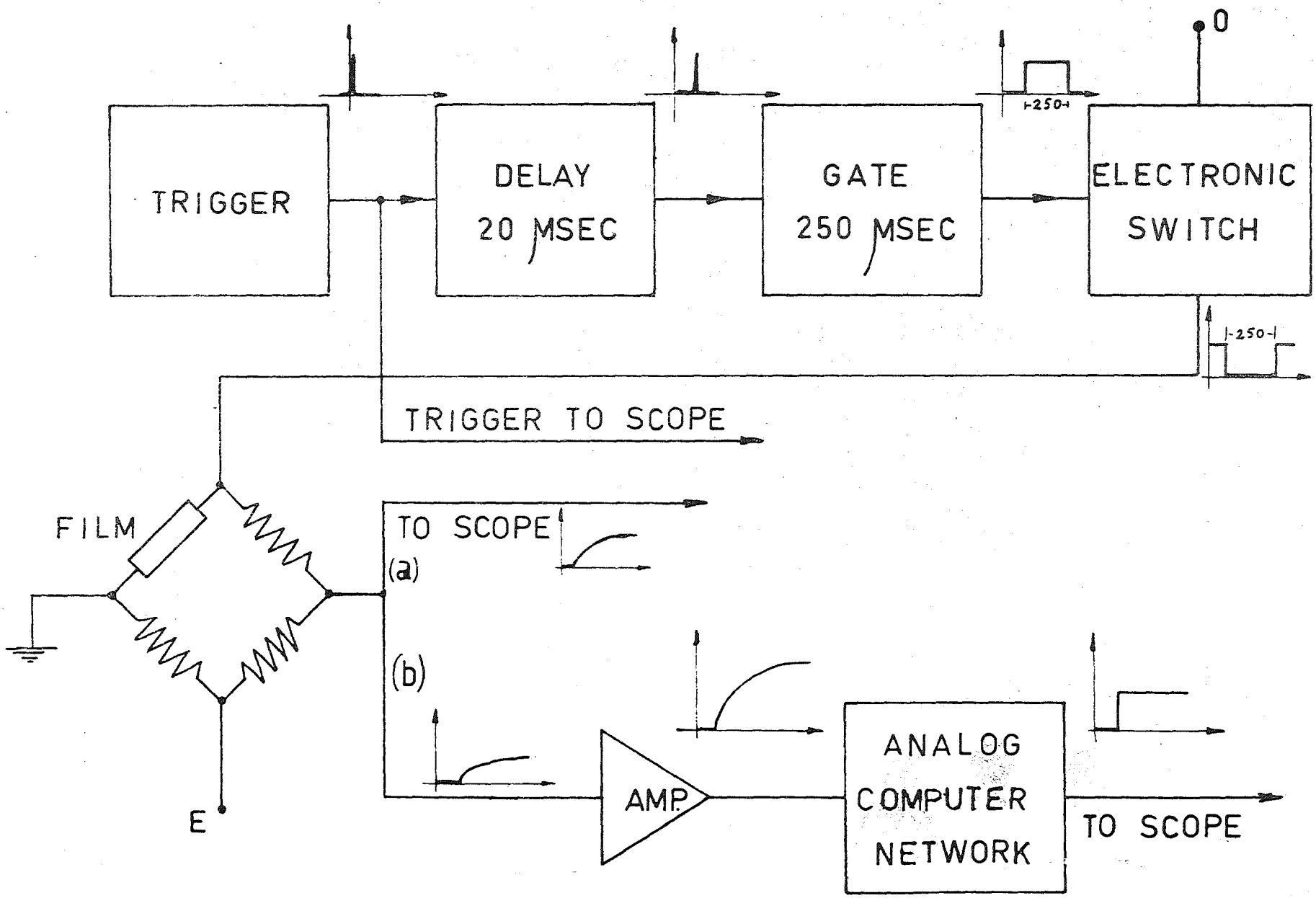

FIG. 26 CALIBRATION CIRCUIT BLOCK DIAGRAM

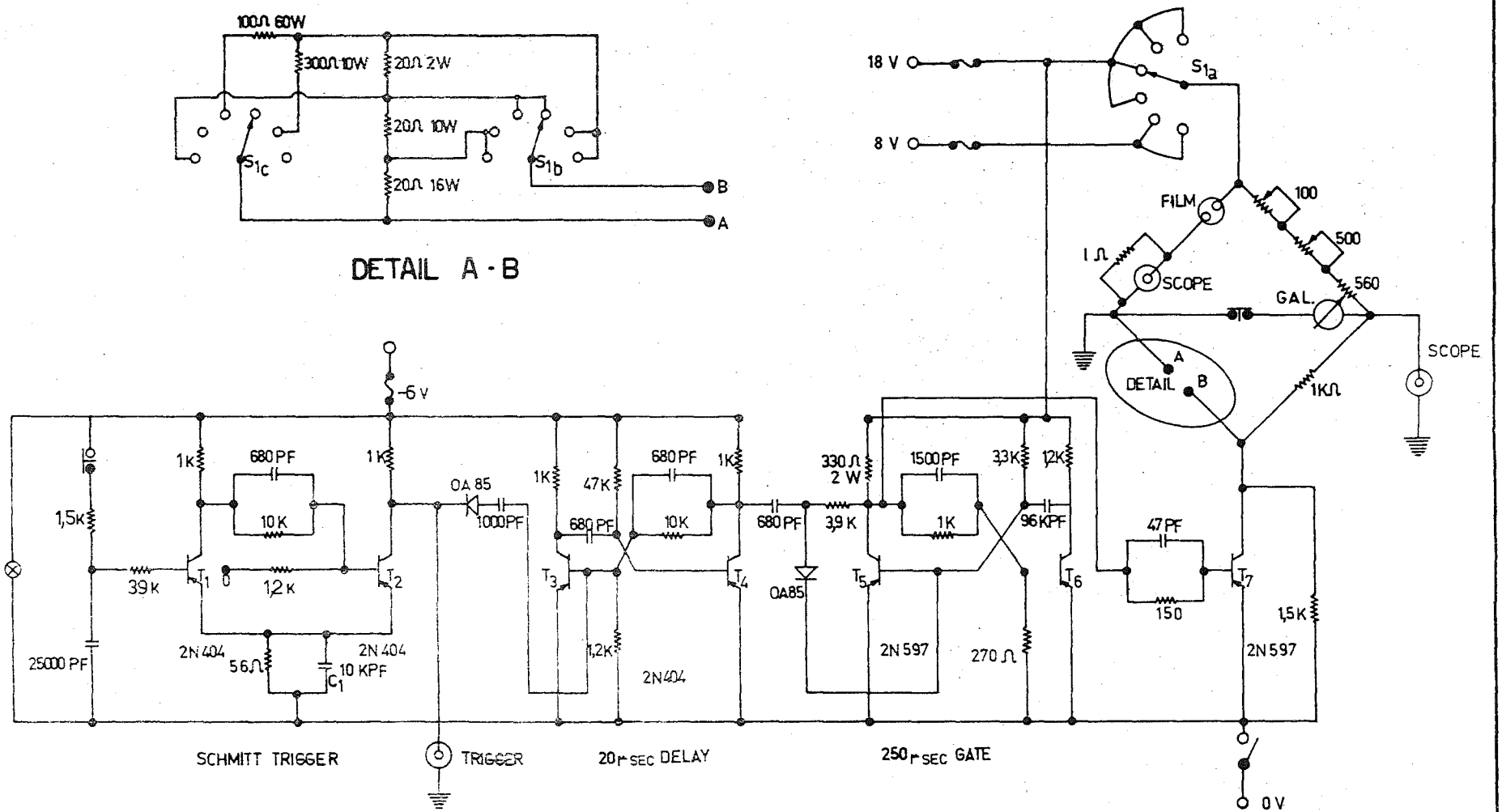

FIG. 27 CALIBRATION CIRCUIT

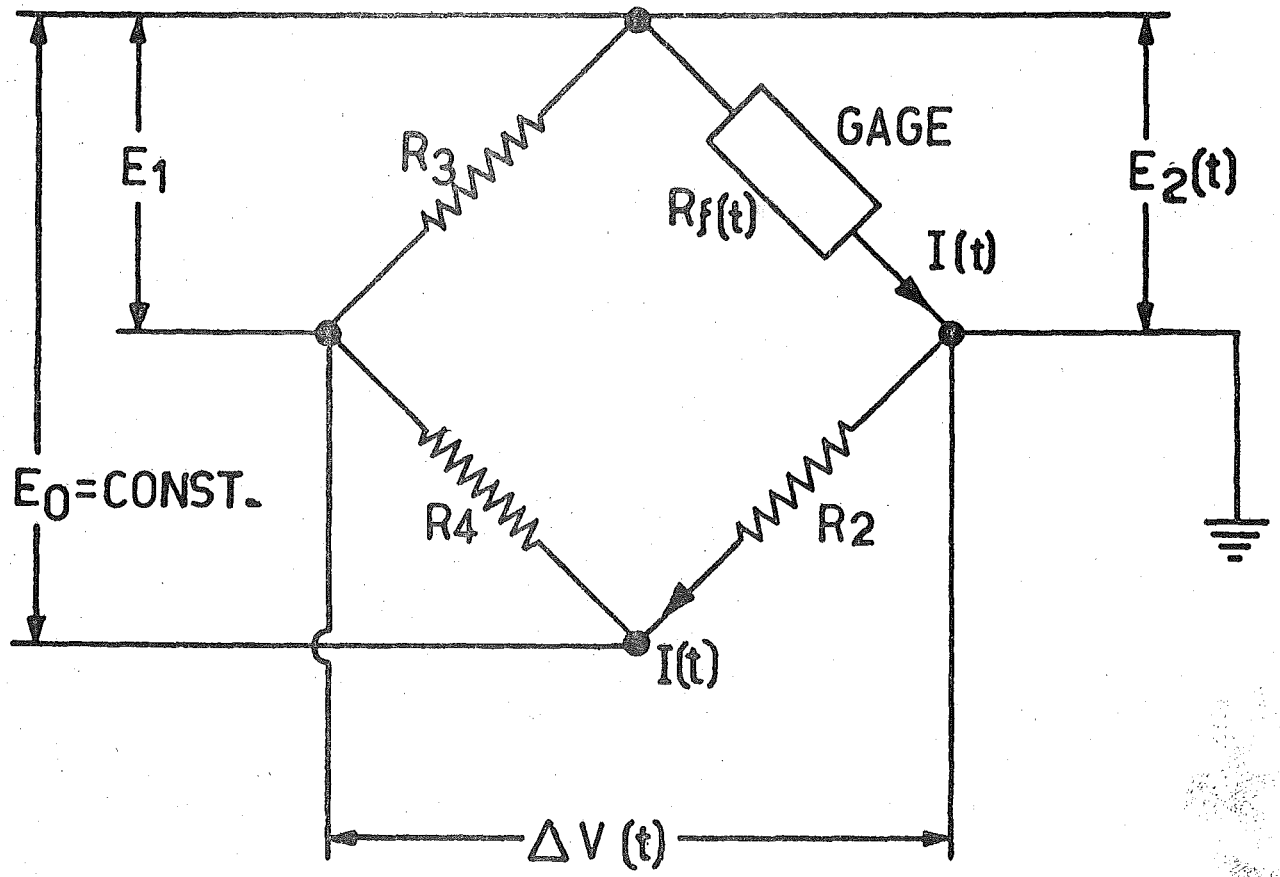

FIG. 28 BALANCING BRIDGE

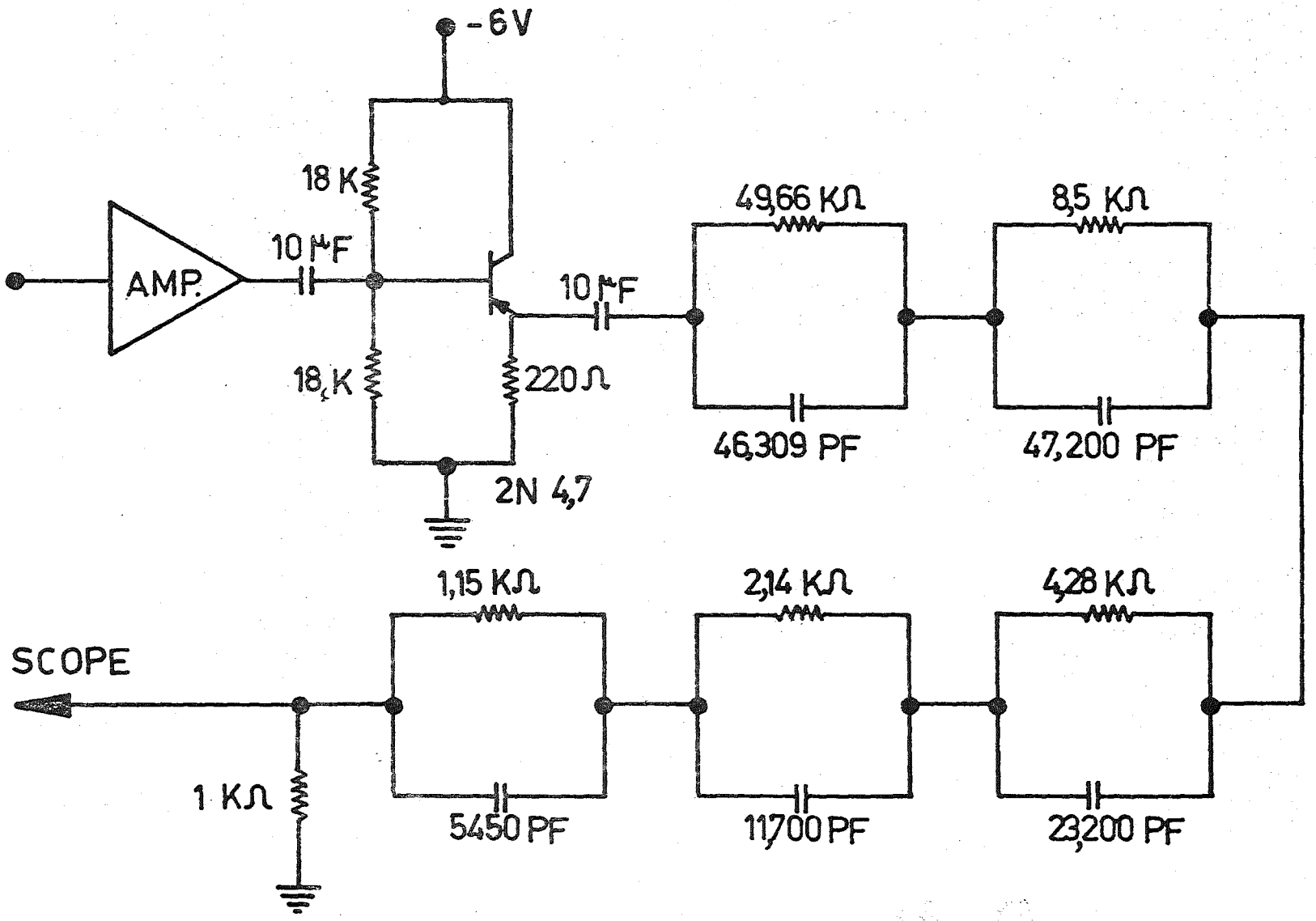

FIG. 29 ANALOG NETWORK

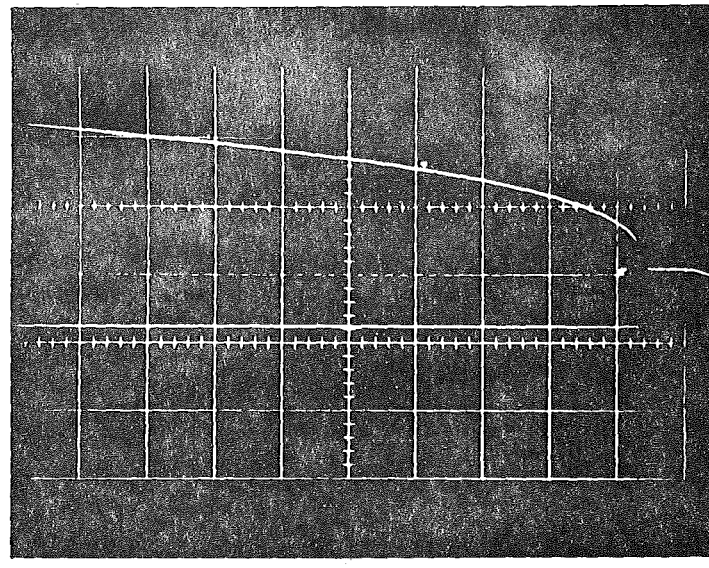

FILM RESISTANCE = 13.01 OHM
SENSITIVITY : UPPER TRACE 20 mV/DIV.
LOWER TRACE 100 mV/DIV.
SWEEP : 20 μsec/DIV.

FIG. 30 CALIBRATION CIRCUIT OUTPUT SIGNAL

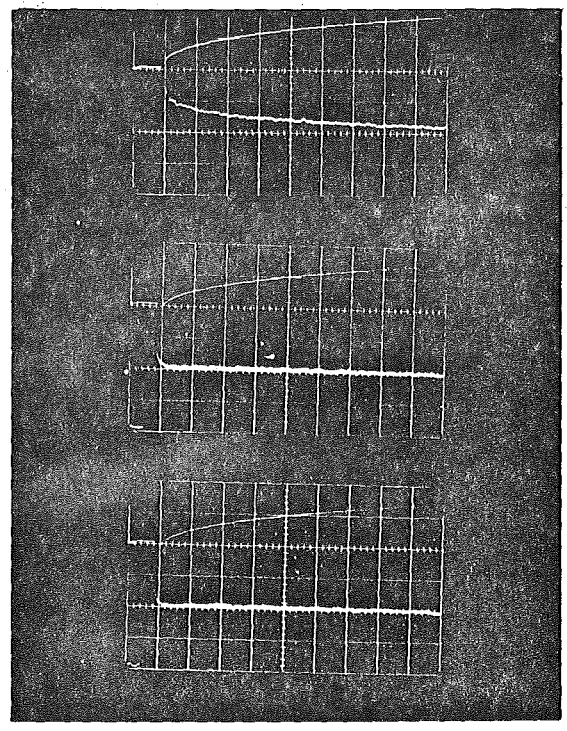

FILM RESISTANCE = 29.45 OHM
SENSITIVITY : 50 mV/DIV.
SWEEP : 20 μsec/DIV.

FIG. 31 ANALOG NETWORK CALIBRATION SIGNAL